Nanoscale

ROYAL SOCIETY OF CHEMISTRY

MINIREVIEW

View Article Online
View Journal | View Issue



Cite this: *Nanoscale*, 2024, **16**, 4542

# Recent progress of high-performance in-plane zinc ion hybrid micro-supercapacitors: design, achievements, and challenges

Wenwen Liu, * Hongling Li and Roland Yingjie Tay *

With the increasing demand for wearable and miniature electronics, in-plane zinc (Zn) ion hybrid micro-supercapacitors (ZIHMSCs), as a promising and compatible energy power source, have attracted tremendous attention due to their unique merits. Despite enormous development and breakthroughs in this field, there is still a lack of a systematic and comprehensive review to update the recent progress of in-plane ZIHMSCs in the design and fabrication of both micro-anodes and micro-cathodes, the exploration and optimization of new electrolytes, and the investigation of related-energy storage mechanisms. This minireview summarizes the key breakthroughs and recent advances in the construction of high-performance in-plane ZIHMSCs. First, the background and fundamentals of in-plane ZIHMSCs are briefly introduced. Then, new concepts, strategies, and latest exciting developments in the preparation and interfacial engineering of Zn metal micro-anodes, the fabrication of advanced micro-cathodes, and the exploration of new electrolyte systems are discussed, respectively. Finally, the key challenges and future directions for the development of high-performance in-plane ZIHMSCs are presented as well. This review not only accounts for the recent research progress in the field of the in-plane ZIHMSCs, but also provides important new insights into the design of next-generation miniaturized energy storage devices.

Received 30th November 2023,
Accepted 4th January 2024

DOI: 10.1039/d3nr06120e

rsc.li/nanoscale



## 1. Introduction

The rapid expansion of wearable/portable electronic devices, implantable medical sensors, and Internet of Things has stimulated the booming development of microelectrochemical energy storage devices.[1–7] Conventional energy storage systems

*School of Electrical and Electronic Engineering, Nanyang Technological University, 50 Nanyang Avenue, Singapore 639798, Singapore. E-mail: wenwen.liu@ntu.edu.sg, rolandtay@ntu.edu.sg*

**Wenwen Liu**

*Wenwen Liu is currently a senior research fellow in Nanyang Technological University. He received his Ph.D. degree in Chemical Engineering in 2020 from the University of Waterloo. Before joining Nanyang Technological University, he was a research scientist at the A*STAR Institute of Materials and Research Engineering from 2020 to 2023. His research mainly focuses on the development of advanced functional materials for electrochemical energy storage and conversion applications, such as supercapacitors, lithium-ion batteries, metal–air batteries, and water splitting.*

**Hongling Li**

*Hongling Li received her Ph.D. degree at the College of Chemistry and Chemical Engineering from Lanzhou University in 2012. She is currently a senior research fellow in the School of Electrical and Electronic Engineering at Nanyang Technological University (NTU). Her current research interest focuses on advanced low-dimensional materials such as graphene, boron nitride and their polymer composites, as well as their energy storage and thermal management applications in various modern electronic devices and systems.*

usually have obvious shortcomings (*e.g.*, large volume, heavy weight, and inferior flexibility) and cannot be used as effective power sources to meet new demands.[8–10] To address these issues, much effort has been devoted to developing compatible and miniaturized energy storage devices. Among various reported miniaturized energy storage systems,[11–14] micro-supercapacitors (MSCs) have attracted tremendous interest as compared to micro-batteries due to their unique merits such as fast charge/discharge capability, high power density, long cycling durability, and availability in various shapes.[15–21] Unfortunately, MSCs possess relatively low energy density, which limits their large-scale applications, especially in the field of wearable/portable electronic devices. As an attractive alternative, hybrid micro-supercapacitors (HMSCs) have been proposed as a new concept that combines the respective advantages of micro-batteries and MSCs, in which a battery-type electrode with redox reaction works as an energy source and a capacitor-type electrode serves as a power source.[22–26] Therefore, the HMSCs with rationally designed electrodes and configuration can couple well the merits of micro-batteries and MSCs, and make the best use of both devices' characteristics, thus enabling the obtained device to achieve excellent electrochemical performance.

So far, HMSCs based on monovalent metal ions (*e.g.*, $Li^+$, $Na^+$, and $K^+$) have been widely reported,[27–31] while multivalent metal ion based HMSCs (*e.g.*, $Zn^{2+}$, $Ca^{2+}$, and $Al^{3+}$) have received limited attention.[27,32,33] Among the previously reported multivalent metal-ion HMSCs, Zn ion HMSCs (ZIHMSCs) with great potential to generate high energy density without compromising other properties have specially captured increasing attention.[34–38] Generally, the ZIHMSCs can be divided into three categories based on their configurations: in-plane, fiber, and sandwich types.[2,25,39–41] Particularly, the in-plane ZIHMSCs composed of separated parallel cathode and anode electrodes on a single substrate have garnered great interest. This is because of their attractive advantages such as fast ion diffusion, small internal resistance, and being free of a separator, which in turn enable the obtained device with ultra-high rate capability, fast frequency response capability, and high-power density.[20,42,43] However, the research on the design and development of in-plane ZIHMSCs is still in its infancy. As such, a systematic and comprehensive review with special emphasis on the new concept and design strategies for both micro-anodes and micro-cathodes as well as the exploration and optimization of electrolytes is highly desirable, which could be a useful and important up-to-date guidance for the future development of ZIHMSCs.

Herein, it should be mentioned that although the in-plane ZIHMSCs are divided into two categories based on the electrode materials and configurations, the in-plane ZIHMSCs discussed in this minireview only refer to the device assembled with the metallic Zn micro-anode. Such considerations are mainly based on the clarity of the logical structure of this minireview and its limited length, as well as the attractive advantages of metallic Zn micro-anodes that feature high theoretical capacity (820 mA h $g^{-1}$), low redox potential (−0.76 V *vs.* standard hydrogen electrode), high conductivity, easy handling, and high safety.[2,15,44] Therefore, the configuration of in-plane ZIHMSCs presented here is constructed by metallic Zn micro-anodes and capacitor-type micro-cathodes unless specified otherwise. In this minireview, we systematically assess the recent progress in the field of in-plane ZIHMSCs. First, the basic information and principles related to the in-plane ZIHMSCs are briefly summarized. Then, new strategies for the design and preparation of metallic Zn micro-anodes, micro-cathodes, and advanced functional electrolytes as well as their latest exciting developments are highlighted. Finally, a summary and outlook on recent in-plane ZIHMSCs are presented. We believe that this review would attract more and more attention from researchers to this new direction and thus promote its further development and even practical applications.

**Roland Yingjie Tay**

*Roland Yingjie Tay is an assistant professor in the School of Electrical and Electronic Engineering (EEE) at Nanyang Technological University (NTU). He received his B.Eng. and Ph.D. in EEE from NTU in 2009 and 2016, respectively. In 2021, he was awarded the International Postdoctoral Fellowship (IPF) at NTU and did his postdoctoral fellowship at California Institute of Technology (Caltech). His research focuses on the synthesis and development of low-dimensional nanomaterials and employing them for various applications including thermal management, electromagnetic interference shielding, flexible electronics, energy and sensor devices, and materials for harsh environments.*

## 2. Fundamentals of in-plane ZIHMSCs

### 2.1 Operation principles of in-plane ZIHMSCs

In-plane ZIHMSCs presented here are a hybrid energy storage device composed of a battery-type Zn micro-anode, a capacitor-type micro-cathode, and electrolyte (Fig. 1a). Note that the Zn micro-anode and the micro-cathode electrodes are parallel and separated by space instead of a separator. Also, the electrolyte, usually consisting of a salt and solvent, is responsible for providing ionic conductivity between the electrodes. Generally, aqueous solutions containing different zinc salts (*e.g.*, $ZnCl_2$, $ZnSO_4$, $Zn(NO_3)_2$, $Zn(CH_3COO)_2$, and $Zn(CF_3SO_3)_2$) are the most popular electrolytes used for the assembly of the device due to their advantages (*e.g.*, high ionic conductivity, low viscosity).[45–47] The operating voltage of aqueous electrolytes is usually in the range of 0.2–1.8 V,[48,49] which is limited by the competitive

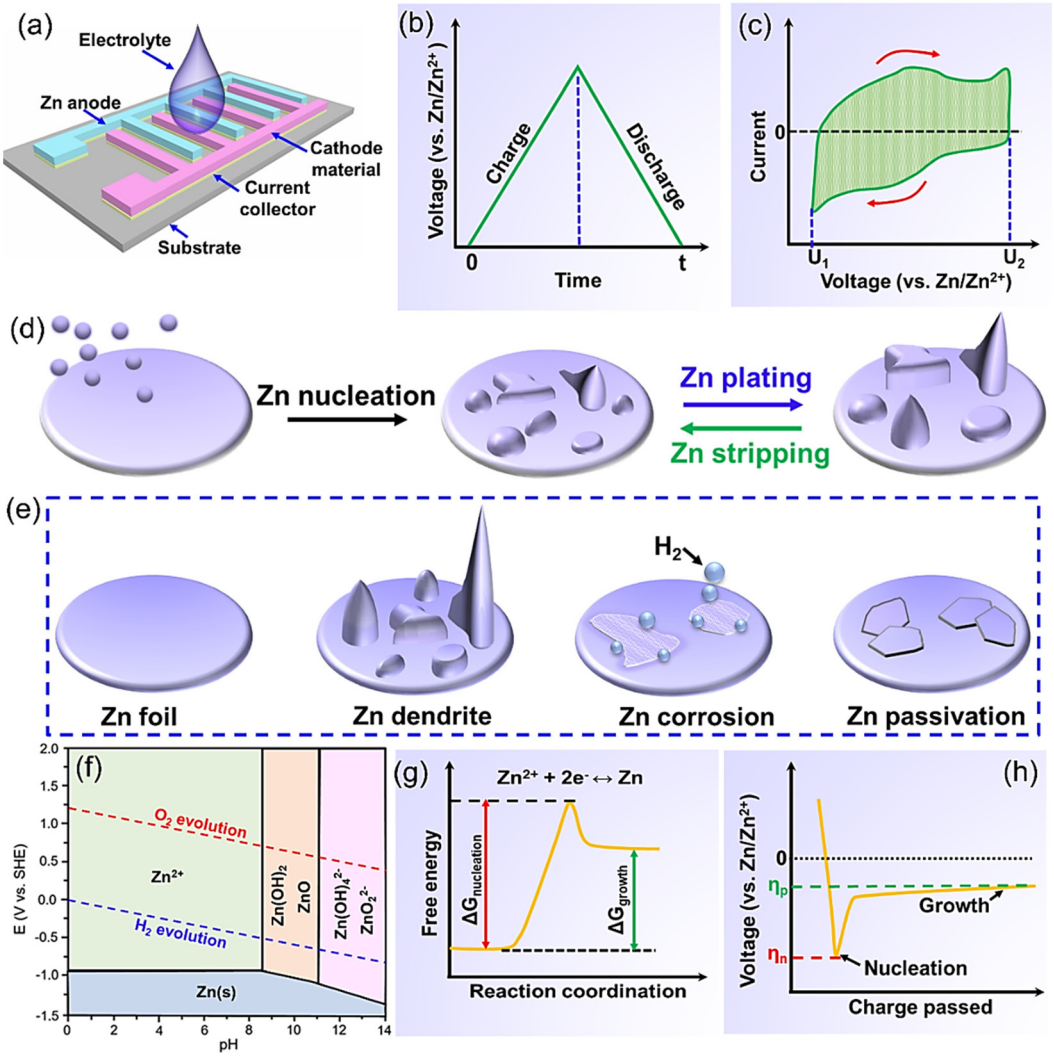


**Fig. 1** (a) Schematic diagram of the components of a typical in-plane ZIHMSC. Evaluation of the specific capacitance of ZIHMSCs based on (b) typical linear charge/discharge curves and (c) CV curves, respectively. (d) Illustration of the Zn dendrite formation and growth during plating/stripping processes. (e) Schematic illustration of dendrites, corrosion, and passivation on Zn foil. (f) Pourbaix diagram of a Zn/$H_2O$ system under different pH values and potentials. (g) Energy barrier for the Zn nucleation process. (h) Voltage profile during the Zn deposition process.

decomposition of water. In this scenario, non-aqueous electrolytes (*e.g.*, organic electrolytes, ionic liquids) are explored to extend the voltage beyond the limitation of 1.8 V.[50,51]

The overall energy storage mechanism of the in-plane ZIHMSCs is based on the fast adsorption/desorption of ions on the surface of the cathode and reversible Zn stripping/plating.[52,53] Specifically, Zn anode loses electrons, and then the generated $Zn^{2+}$ ions move to the electrolyte during the discharge process, while the $Zn^{2+}$ ions are plated on the Zn anode during the charge process. The main reaction occurring on the Zn anode side can be expressed by the eqn (1):

$$Zn - 2e^- \leftrightarrow Zn^{2+} \quad (1)$$

Meanwhile, accompanying side reactions may also occur on the anode side, which can be described by the following eqn (2):

$$4Zn^{2+} + 6OH^- + SO_4{}^{2-} + xH_2O \leftrightarrow Zn_4SO_4(OH)_6 \cdot xH_2O \quad (2)$$

This can reasonably explain why the $Zn_4SO_4(OH)_6{\cdot}xH_2O$ product can be detected on the Zn anode surface,[54,55] which is due to the unstable pH environment of the electrolyte during the charge/discharge process.

For the cathode side, there are still some debates about its energy storage mechanism because of the complicated working mechanism during the charge/discharge process. According to the literature, two possible energy storage mechanisms are proposed as follows:

(a) Physical adsorption/desorption mechanism as shown in eqn (3) and (4):

$$C_{materials} + Zn^{2+} \leftrightarrow C_{materials}||Zn^{2+} \quad (3)$$

 

$$C_{\text{materials}} + X_{\text{anions}}{}^{y-} \leftrightarrow C_{\text{materials}}||X_{\text{anions}}{}^{y-} \quad (4)$$

where $C_{\text{materials}}$ and $X_{\text{anions}}{}^{y-}$ refer to carbon cathode materials without functional groups and the anions (*e.g.*, $SO_4{}^{2-}$, $(CF_3SO_3)^-$) of the electrolytes, respectively. The energy storage mechanism was that $Zn^{2+}$ cations were mainly involved in the adsorption/desorption process on the cathode side, thus contributing to the capacity, while the anions also participated in the formation of an electric double layer before the charge process, and then diffused back into the electrolyte during the discharge process.[56–58]

(b) Chemical adsorption/desorption mechanism as shown in eqn (5) and (6):

$$M_{\text{materials}} \cdots \text{O} + \text{Zn}^{2+} + 2\text{e}^- \leftrightarrow M_{\text{materials}} \cdots \text{O} \cdots \text{Zn} \quad (5)$$

and/or

$$M_{\text{materials}} \cdots \text{O} + \text{H}^+ + \text{e}^- \leftrightarrow M_{\text{materials}} \cdots \text{O} \cdots \text{H} \quad (6)$$

where $M_{\text{materials}}\cdots$O represents the cathode materials (*e.g.*, heteroatom doped carbon, metal oxides/carbides/nitrides) with rich functional groups. Here, this energy storage mechanism is mainly based on the reversible chemical adsorption/desorption of $Zn^{2+}$ and/or $H^+$ ions during the charge/discharge process, where chemical bonding was formed between $Zn^{2+}$ (or $H^+$) ions and the cathode materials.[59,60] There is no doubt that the chemical adsorption/desorption mechanism will enable devices with much higher capacities due to the pseudocapacitive contribution. In addition, some researchers claimed that the adsorption/desorption of anions on the cathode materials were also involved in the process.[61–63]

### 2.2 Electrochemical performance evaluation

The equations for evaluating the specific capacity of conventional supercapacitors also apply to the ZIHMSCs. Therefore, the specific capacitance can be calculated based on cyclic voltammetry (CV) and charge/discharge curves, respectively. Assuming that the charge/discharge curves of the ZIHMSCs show a near-linear relationship with time (Fig. 1b), its specific capacitance ($C$) can be evaluated from the following eqn (7):

$$C = \frac{I \cdot \Delta t}{m \cdot \Delta V} \quad (7)$$

where $I$, $\Delta t$, $m$, and $\Delta V$ are the discharge current, the discharge time, the mass loading of active materials, and the voltage between high potential limit and low potential limit, respectively.

If the charge/discharge curves do not show a linear or near-linear relationship with time, specific capacitance will be overestimated based on the charge/discharge curves. In this case, the specific capacitance ($C$) can be evaluated by the CV curve (Fig. 1c) based on the following eqn (8):

$$C = \frac{\int_{U_1}^{U_2} I(U)\mathrm{d}U}{2v \cdot m \cdot \Delta V} \quad (8)$$

where $U_2$, $U_1$, $\int I(U)\mathrm{d}U$, $m$, and $\Delta V$ are the high potential limit of the CV curve, low potential limit of the CV curve, integrated area surrounded by the CV curve, mass loading of the active materials, and voltage between high potential limit and low potential limit, respectively.

Meanwhile, the corresponding energy density ($E$) and power density ($P$) can be calculated from the following eqn (9) and (10), respectively:

$$E = \frac{C \cdot (U_2^2 - U_1^2)}{2} \quad (9)$$

$$P = \frac{3600 \times E}{\Delta t} \quad (10)$$

where $C$, $U_2$, $U_1$, and $\Delta$t are the specific capacitance, high potential limit, low potential limit, and the discharge time, respectively.

### 2.3 Strategies for high energy and power densities

According to the energy density equation, specific capacitance and cell voltage are two key parameters that determine the energy density of the device. Starting from this point, much effort has been devoted to improving the energy density of the cell based on the following strategies: (a) designing advanced cathode materials with large potential windows;[64,65] (b) enlarging the potential window of the device by adopting suitable/novel electrolyte systems;[44,66] and (c) improving the specific capacitance of cathode materials.[67] To achieve high-power density, feasible approaches mainly focus on the improvement of the sluggish reaction kinetics of the micro-cathode and micro-anode materials by tailoring their physicochemical properties through various surface and structural engineering strategies. With these considerations in mind, this minireview mainly focuses on the exploration and design of high-performance micro-anodes and micro-cathodes as well as properly matched electrolytes accompanied by novel device configuration.

## 3. Properties and progress of metallic Zn micro-anodes

Metallic Zn has been considered as a promising anode material for constructing ZIHMSCs due to its attractive electrochemical characteristics and well-established industrial fabrication technology.[44,68,69] However, metallic Zn anode usually suffers from uncontrolled dendrite growth (Fig. 1d) and other accompanying side reactions (*e.g.*, corrosion, hydrogen evolution reaction) (Fig. 1e), thus resulting in poor electrochemical reversibility, huge capacity decay, low coulombic efficiency, and short-term cycling life in the obtained device.[70] There is no doubt that these existing issues (*e.g.*, Zn dendrites, side reactions) of the metallic Zn anode will lead to the compromised performance of the final device and thus hinder its large-scale practical applications.[2,71] Before tackling these problems of the metallic Zn anode, it is necessary to dig deeper into its electro-chemical properties, which are believed to be helpful for proposing effective strategies.

### 3.1 Chemistry of metallic Zn under different microenvironments

The electrochemical behavior of metallic Zn in aqueous electrolytes is largely affected by the electrolyte conditions and potential (Fig. 1f).[72–77] Notably, there are obvious differences in the existence forms of the metallic Zn anode after electrooxidation (corresponding to the discharge process) under different pH conditions. Note that $Zn^{2+}$ ions are the dominant existence form because a series of reactions are inhibited in a strongly acidic environment (pH < 4),[72] while $ZnO/Zn(OH)_2$ is the main existence form in weakly alkaline environments (8.5 < pH < 11), due to the participation of $OH^-$ in the reaction.[73,74] Further increasing the pH value to a strongly alkaline environment (pH > 12), $Zn(OH)_4^{2-}$ and $ZnO_2^{2-}$ appear and the corresponding solubility significantly decreases as the reactions continue, leading to the loss of active materials and passivation or dendrite growth.[72,74,75] Note that electrolytes that are too acidic or alkaline cannot be considered suitable electrolytes due to the severe corrosion, dendritic growth, and $H_2$ evolution.[76] In comparison, at near-neutral pH levels (4 < pH < 8),[77] the Zn anode mainly adopts a direct reaction pathway to form $Zn^{2+}$ ions upon discharge while no inactive discharge product is generated, thereby making it easy to charge the obtained device. With the assistance of the Pourbaix diagram, the existence forms of the metallic Zn after electrochemical oxidization under different pH levels can be identified, which helps better understand the electrochemical reactions of the Zn anode under different electrolyte conditions.[72]

### 3.2 Issues of metallic Zn anodes and potential risks

Like aqueous Zn-ion batteries and Zn-ion capacitors,[74–76] the metallic Zn micro-anodes used in ZIHMSCs have similar issues such as Zn dendrite, hydrogen evolution, and corrosion. The main reasons for Zn dendrite formation and growth are non-uniform Zn dissolution and uneven deposition during the discharge/charge process (Fig. 1d). Briefly, $Zn^{2+}$ ions tend to accumulate on the protrusions with a large curvature than on a flat surface because the former requires smaller free energy (or overpotential) to form a new stable nucleus (Fig. 1g and h).[74] This accelerates dendrite formation and growth in neutral/mildly acidic electrolytes during the repetitive charge/discharge process, thus leading to capacity decay.[74] Even worse, the continuous growth of dendrites will penetrate the separator at some point, causing a short circuit of the device. Furthermore, the generated irreversible products precipitated on the Zn anode surface reduce the Zn anode/electrolyte interface and block the subsequent ion diffusion and deposition to some extent, thereby resulting in poor rate capability and high irreversible capacity loss.[74]

According to the Pourbaix diagram (Fig. 1f), the hydrogen evolution reaction (HER) is a competitive reaction against Zn plating over the entire pH range. In other words, the HER is an inevitable side reaction in the Zn plating process, thus resulting in the coulombic efficiency of the Zn plating process to be less than 100%. Furthermore, the HER side reaction can also cause cell swelling and other safety issues. Besides, metallic Zn is usually active in aqueous electrolytes from the thermodynamic perspective, so there are some side reactions that occur at the Zn/electrolyte interface. Among them, Zn corrosion is one of the common side reactions, but ongoing Zn corrosion reaction and continuous consumption of Zn electrode and electrolytes will result in a limited shelf-life of the device. Also, corrosion can create an uneven surface on the Zn anode, which accelerates the dendrite formation and growth, and consequently reduces the coulombic efficiency. Note that these three issues, including dendrites, corrosion, and HER, are closely interrelated, and mutually reinforce each other. Undoubtedly, if these three issues can be addressed by appropriate strategies, it will be beneficial for the design of high-performance ZIHMSCs.

### 3.3 Preparation and interfacial engineering of Zn micro-anodes

From our point of view, obtaining dendrite-free and stable metallic Zn micro-anodes is very important for constructing high-performance ZIHMSCs. To suppress Zn dendrites and avoid related side reactions, the key point is to control the nucleation and growth process through surface and structure engineering of the Zn micro-anodes. As reported, Zn nucleation and growth process mainly rely on several crucial factors (*e.g.*, the number of nucleation sites, nucleation barrier),[75,76,78] which are closely related to the specific area, zincphilicity, and crystal structure and orientation of the Zn anode.[79,80] Therefore, researchers are inspired to regulate the zinc metal/electrolyte interface through different strategies (*e.g.*, architecture engineering, surface modification, introduction of electrolyte additives, adoption of high-concentration electrolytes) to induce homogeneous zinc nucleation and growth, thus achieving dendrite-free and stable Zn micro-anodes.[76,79,80] Currently, Zn micro-anodes mainly exist in the following three forms: Zn powder-derived electrodes, Zn foil/plate electrodes, and 3D architecture Zn electrodes.[1,76,81–84] The selection of the suitable form and structure of Zn micro-anodes largely depends on the configuration of the ZIHMSCs and its potential applications. In this section, the progress including new concept, strategies, and technologies for designing and constructing high-performance Zn micro-anodes through different interfacial engineering strategies are thoroughly summarized and discussed.

The morphology and structure of Zn micro-anodes can enable them to show different dissolution rates and crystal planes exposed, thereby having a direct effect on their electrochemical performance.[1,69,81] Therefore, regulating the morphology and architecture of the Zn micro-anodes is a very effective strategy to achieve Zn micro-anodes with high-performance. In this regard, more and more researchers have begun to explore new advanced techniques (*e.g.*, laser cutting, spray-coating, and electrochemical plating) to design and prepare metallic Zn micro-anodes with specific morphologies and unique structures. Among the different existence forms of Zn micro-anodes, the Zn powder-based micro-anode as a com-

 

monly used zinc anode has shown great potential in the field of ZIHMSCs, especially when considering large-scale applications, due to its high utilization rate, tunable surface area, low cost, and easy storage.[84–86] However, zinc powder cannot be directly used as a micro-anode electrode to assemble the ZIHMSCs. Therefore, it is necessary to explore simple and feasible processing methods to construct the micro-anode electrode based on zinc powder.

Encouragingly, a Zn micro-anode interdigital electrode was fabricated by uniformly spray-coating Zn powder dispersion (Zn power/PVDF/DMF mixture) onto the conductive substrate with the assistance of masks.[87] Meanwhile, various printing technologies (*e.g.*, inkjet printing, 3D printing, and screen-printing) have been employed to prepare Zn micro-anodes due to their unique advantages.[88–90] Among them, the 3D printing technique, as a revolutionary manufacturing method, is widely used in the design and preparation of electrodes due to its controllable geometry and unique architecture as well as low cost. Based on its unique advantages, it has been adopted to design Zn micro-anodes. For example, Li *et al.* used a direct ink writing 3D printer to construct a Zn micro-anode with many channels and pores (Fig. 2a–c),[88] which could effectively suppress Zn dendrite formation and facilitate access to the electrolyte. Although 3D printing technology is impressive, there are still some issues that need to be addressed, such as cracking and low utilization of active materials, especially the high-thickness electrodes. In this case, Lu *et al.* attempted to solve these problems by exploring new ink formulations and optimizing the printing parameters (Fig. 2d),[89] thus achieving a satisfactory Zn micro-anode. It is worth noting that Zn nanospheres are encapsulated by CNTs with conductive additives and form a 3D network structure (Fig. 2e and f), which improves the conductivity and favors charge transfer. Also, the printed Zn micro-anode can withstand different bending conditions, indicating its robust durability. In addition, screen-printing is another promising technique for the fabrication of the Zn micro-anode because it is not only feasible to design the electrode on various substrates, but is also a low-cost and large-scale technique. To further demonstrate this concept, Wang *et al.* used a screen-printing technique to construct the Zn micro-anode (Fig. 2g).[90] Note that Zn powder-based ink is successfully deposited on the graphene-based interdigital planar patterns (Fig. 2h and i). Encouragingly, the Zn micro-anode can be prepared on different substrates such as cloth, paper, and glass, indicating the universality of this technique.

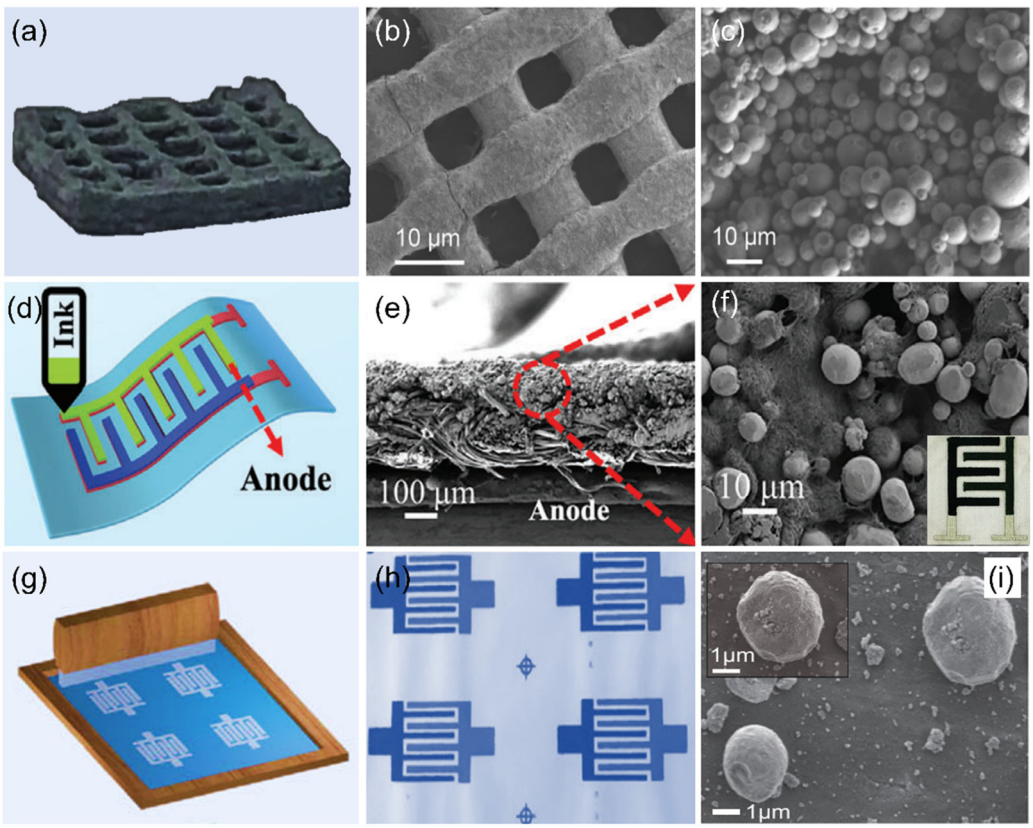


**Fig. 2** (a) Digital photograph of a Zn micro-anode prepared by a 3D printing technique and its corresponding (b) low- and (c) high-magnification SEM images. Reproduced with permission from ref. 88. Copyright 2022, Elsevier. (d) Illustration of a Zn micro-anode fabricated by a modified 3D printing technique and its corresponding cross-sectional SEM images at (e) low- and (f) high-magnification. Reproduced with permission from ref. 89. Copyright 2023, WILEY-VCH. (g) Schematic diagram of a Zn micro-anode prepared by a screen-printing technique, (h) obtained interdigitated patterns, and (i) the corresponding SEM image. Reproduced with permission from ref. 90. Copyright 2020, Oxford University Press.

Furthermore, Zn foil/plate is another alternative anode electrode because the direct use of commercial Zn foil as both anode electrode and current collector is simple and easy-to-handle as well as avoids the complicated manufacturing process.[76,82] With these attractive advantages, a Zn micro-anode was prepared by laser cutting of zinc foil (Fig. 3a) and acted as an electrode material of the ZIHMSC device.[83] In addition, the development and construction of 3D structured Zn micro-anodes is an effective and attractive strategy to suppress dendrite growth and improve device performance.[1,27,76] Since 3D Zn metal anode has a large specific surface area and good conductivity, which can provide rich active nucleation sites, increase the contact area with the electrolyte, lower interfacial transmission resistance, and reduce current density, thus suppressing dendrite growth, increasing active material utilization, and favoring deep discharge.[76,91] Among the different methods, electrochemical plating methods (*e.g.*, cyclic voltammetry route, potentiostatic approach, galvanostatic technique) have attracted tremendous attention for constructing 3D Zn metal micro-electrodes. This is because it is not only an efficient, high-resolution, and mask-free approach, but also a method with simple-processing and low-cost. Importantly, some key factors (*e.g.*, electrolyte type, substrate, applied technology, current density, and time) adopted during zinc electroplating strongly influence the adsorption energy of Zn atoms, nucleation barriers, and crystal orientation, thus resulting in morphology and structure differences of zinc micro-anodes. Notably, a typical 3D Zn anode was obtained using the cyclic voltammetry technique at a scan rate of 50 mV $s^{-1}$ in a three-electrode system,[1] in which two CNT micro-electrodes served as the working and reference electrodes, respectively. After electroplating, the resulting Zn nanosheets were

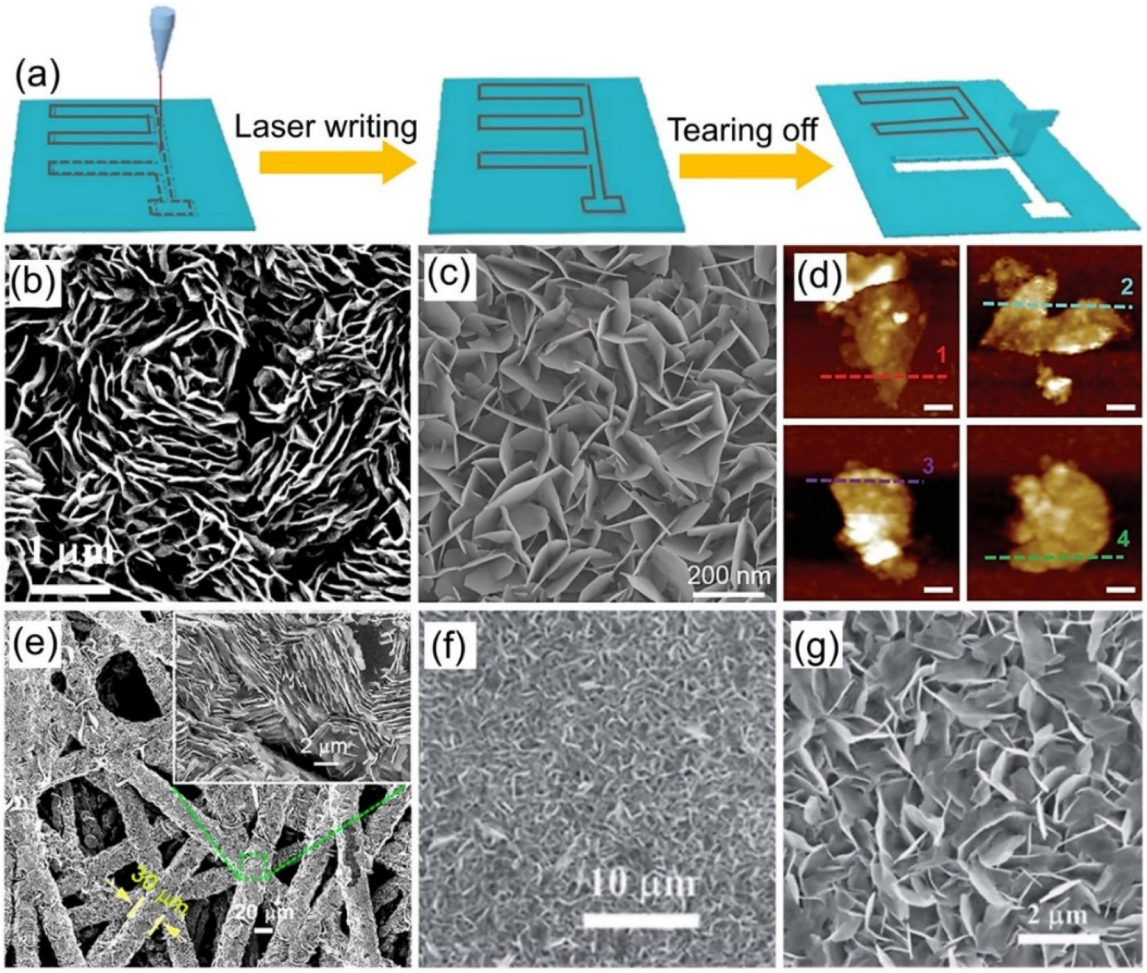


**Fig. 3** (a) Illustration of the fabrication process of a Zn micro-anode by laser cutting. Reproduced with permission from ref. 83. Copyright 2022, American Chemical Society. (b) SEM image of a 3D Zn micro-anode prepared by cyclic voltammetry technique. Reproduced with permission from ref. 1. Copyright 2018, The Royal Society of Chemistry. SEM (c) and AFM (d) images of a 3D Zn anode fabricated using a potentiostatic technique. Reproduced with permission from ref. 27. Copyright 2019, WILEY-VCH. (e) SEM image of Zn grown on carbon fiber prepared using a potentiostatic technique. Reproduced with permission from ref. 92. Copyright 2019, American Chemical Society. (f and g) Low- and high-magnification SEM images of a Zn anode synthesized by a galvanostatic technique. Reproduced with permission from ref. 93. Copyright 2022, The Royal Society of Chemistry.

 

almost vertically grown on the electrode and interconnected with each other to form a 3D structure (Fig. 3b). Undoubtedly, this vertical structure not only favored the electron transfer, but also facilitated the access to the electrolyte and ion diffusion during the charge/discharge processes.[1] By employing the potentiostatic technique, a vertical 3D Zn anode was uniformly grown on the surface of gold interdigital finger electrodes (Fig. 3c and d).[27] Note that the 3D Zn nanosheet anode with a special porous structure not only maintained the similar morphology of the original nanosheets well and no other new phase (*e.g.*, ZnO) was observed after the durability test, but also effectively inhibited Zn dendrite growth. These results demonstrated that the resulting vertical 3D Zn micro-anode possessed excellent reversibility during the stripping/plating processes.[27] With a similar technique, a 3D Zn micro-anode with a thickness of 11 μm was electrodeposited on carbon paper-based finger electrodes (Fig. 3e).[92] The obtained Zn micro-electrode with a unique morphology and architecture exhibited high reversibility of $Zn^{2+}$ stripping/plating. As another representative example, a 3D Zn micro-anode was electrodeposited on an interdigitated Au electrode using a galvanostatic technique (50 mA $cm^{-2}$) in a two-electrode system, where Zn foil and 2 M aqueous $ZnSO_4$ solution were used as the counter electrode and electrolyte, respectively.[93] It was observed that the Zn nanosheets were not only homogeneously deposited on the Au finger electrodes, but also interacted with each other and formed numerous porous networks (Fig. 3f and g). Based on the above discussion, it is reasonable to conclude that the 3D structural micro-anode obtained by different electrochemical plating techniques can effectively induce uniform Zn plating/stripping processes, thus enhancing the durability of the Zn anode as well as the cycling stability of the device.

## 4. Design and construction of advanced micro-cathodes

As a key component, functional micro-cathodes play the most important roles on the electrochemical performance of the ZIHMSCs. Note that there is a specific capacity mismatch between the cathode and Zn metal anode because of different charge storage mechanisms.[92,94] Based on the "wooden barrel theory", the overall performance of the ZIHMSCs, especially the energy density, is obviously limited by the relatively low specific capacity of the micro-cathode. Therefore, it has become urgent to design and fabricate high-performance micro-cathode materials. To date, a variety of cathode materials have been employed to construct high-performance ZIHMSCs due to their multiple advantages such as high specific surface area, unique electronic properties, and easy fabrication.[1,47,93,95]

### 4.1 Carbon-based micro-cathodes

Among various cathode materials, carbon materials (*e.g.*, carbon nanotubes (CNTs), graphene, and activated carbon (AC)) are the most widely explored and adopted cathode materials in the ZIHMSCs due to their various advantages such as light weight, unique stability, high specific surface area and excellent electrical conductivity.[96,97] For the first time, a simple method was reported to prepare a capacity-recoverable ZIHMSC by integrating a capacitor-type CNT micro-cathode and a battery-type zinc micro-anode (Fig. 4a–c).[1] Interestingly, the resulting in-plane ZIHMSCs constructed with a CNT-based interdigitated cathode prepared by laser engraving of CNT paper exhibited high area capacitance (83.2 mF $cm^{-2}$ at 1 mA $cm^{-2}$), high energy density (29.6 μW h $cm^{-2}$), high power density (8 mW $cm^{-2}$), excellent flexibility, and good cycling performance (Fig. 4d).

Apart from CNTs, AC is another kind of suitable candidate for cathode materials owing to its remarkable characteristics such as unique morphology, various porosity, large surface area, and high electric conductivity.[27,47] For example, a new type of ZIHMSC was constructed by employing the capacitor-type AC as the micro-cathode and the battery-type electrodeposited Zn nanosheet as the micro-anode (Fig. 4e).[27] Owing to the fast ion adsorption/desorption on the cathode and the reversible Zn stripping/plating on the anode (Fig. 4f), the as-prepared ZIHMSCs showed outstanding areal capacitance of 1297 mF $cm^{-2}$ at 0.16 mA $cm^{-2}$ (Fig. 4g), ultrahigh areal energy density of 115.4 μW h $cm^{-2}$ at 0.16 mW $cm^{-2}$, and long-term durability (~100% capacitance retention after 10 000 cycles) as well as potential application as power source for electronic devices (Fig. 4h). Furthermore, it was noted that the capacitor behavior of the ZIHMSCs can be improved by coating a pseudocapacitive polymer, poly(3,3′-dihydroxybenzidine, DHB), onto the surfaces of porous AC granules.[92] By combining the poly(3,3′-DHB)/AC composite micro-cathode and Zn micro-anode, the obtained cell showed high areal capacitance (1.1 F $cm^{-2}$), high energy density (150 μW h $cm^{-2}$), and remarkable capacity retention (80% after 3000 cycles). Interestingly, an edible and nutritive ZIHMSC was developed by the assembly of edible AC/Au as the micro-cathode, Zn foil as the micro-anode and $ZnSO_4$ gel as the electrolyte.[83] The edible microdevice exhibited excellent flexibility, good shape adaptability, high biocompatibility and safety as well as outstanding areal capacitance of 605 mF $cm^{-2}$ and high energy density of 215.1 μW h $cm^{-2}$, which holds great promise for biomedical applications.

Besides, graphene (*e.g.*, exfoliated graphene (EG), laser-induced graphene (LIG)) has also been considered another promising alternative cathode material due to its attractive advantages.[47] However, graphene as the cathode material usually suffers from low energy density, which in turn limits its further practical applications. To address this issue, several effective strategies, including integration of graphene with other materials possessing high capacitance and introduction of heteroatom dopants (such as O and F) onto the graphene layer, have been demonstrated in recent years.[98–100] For example, a facile method was adopted to construct free-standing ZIHMSCs with good electrical conductivity by the self-assembly of EG/PANI film without additional conductive addi-

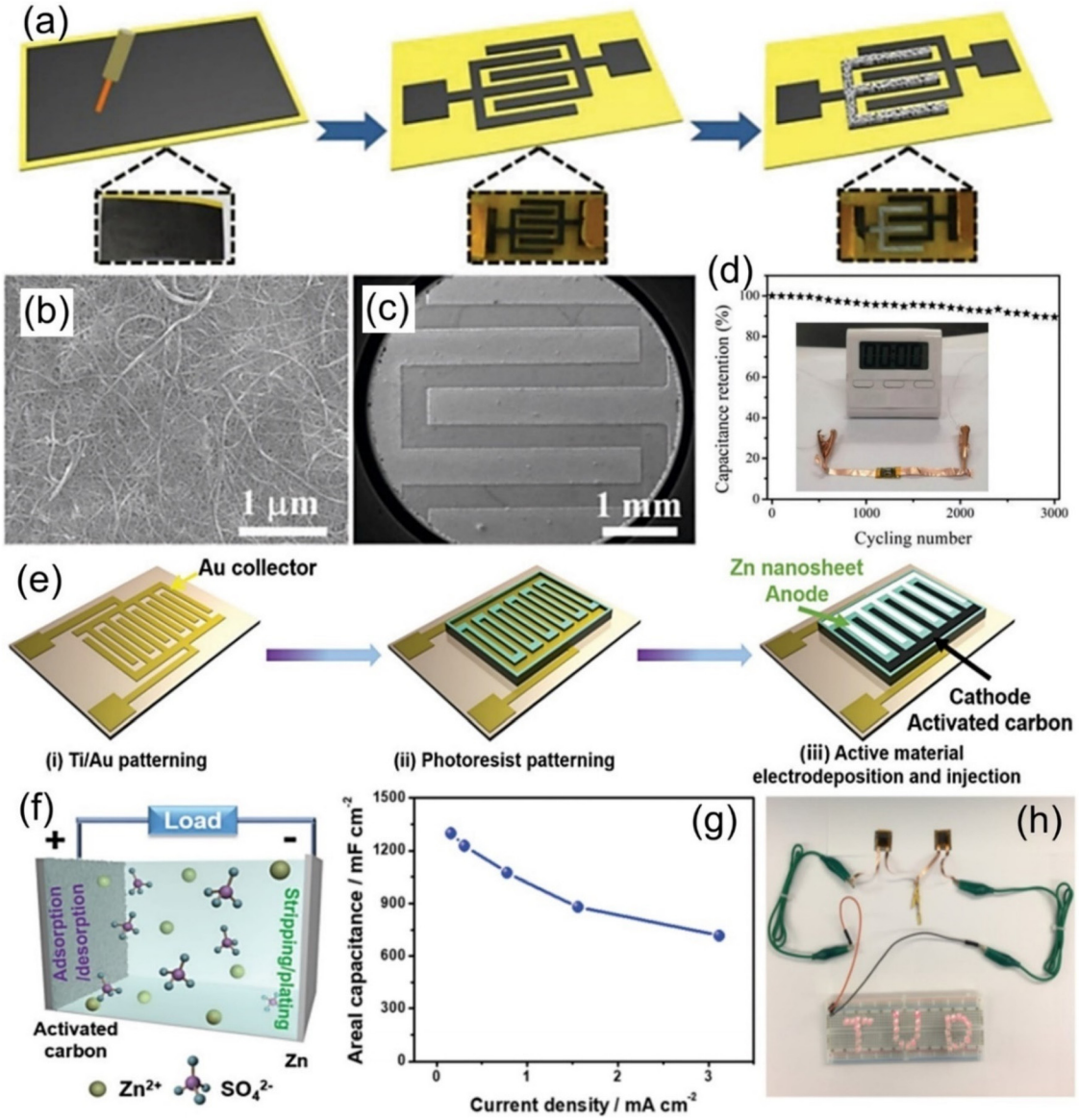


**Fig. 4** (a) Illustration of the fabrication process of the ZIHMSCs based on laser engraving and electrochemical deposition. SEM images of (b) pristine CNT paper and (c) microelectrode after laser engraving. (d) Capacitance retention of the corresponding ZIHMSCs during many bending cycles. Inset in (d) is the photograph of a timer powered by the ZIHMSCs. Reproduced with permission from ref. 1. Copyright 2018, The Royal Society of Chemistry. (e) Illustration of the fabrication process of the ZIHMSCs based on an active carbon micro-cathode and Zn micro-anode. (f) Energy storage mechanism of corresponding ZIHMSCs during the charge/discharge process. (g) Corresponding areal capacitance under different current densities. (h) Demonstration of two ZIHMSCs connected in series powering an LED array. Reproduced with permission from ref. 27. Copyright 2019, WILEY-VCH.

tives or current collectors (Fig. 5a).[98] Owing to the O-containing functional groups on the EG and the effective dispersion of the rod-like PANI fibers in the 2D graphene layer, the achieved EG/PANI film as the interdigitated electrode of the ZIHMSCs displayed ultrahigh capacitance of 1.8 F $cm^{-2}$ at 2.6 mA $cm^{-2}$ and excellent energy density of 755.8 μW h $cm^{-2}$ at 2.3 mW $cm^{-2}$. As another representative example, a flexible ZIHMSC was fabricated by mask-assisted ion sputtering and microelectrode deposition of a PPy/reduced graphene oxide (rGO) hybrid framework cathode and Zn nanosheet anode onto a flexible substrate (Fig. 5b), respectively.[93] The as-fabricated ZIHMSCs delivered high areal capacitance (92.5 mF $cm^{-2}$), high areal energy density (25.2 mW h $cm^{-2}$), moderate voltage window (1.6 V), and outstanding cycling stability (92% capacitance retention after 10 000 cycles), which showed great promise for future flexible self-powered energy systems.[93] In addition, it was noted that *in situ* electrodeposition of polypyrrole (PPy) onto three-dimensional (3D) porous LIG (LIG@PPy) (Fig. 5c) can effectively improve the charge storage capacity and conductivity of the LIG skeleton while maintaining the

 

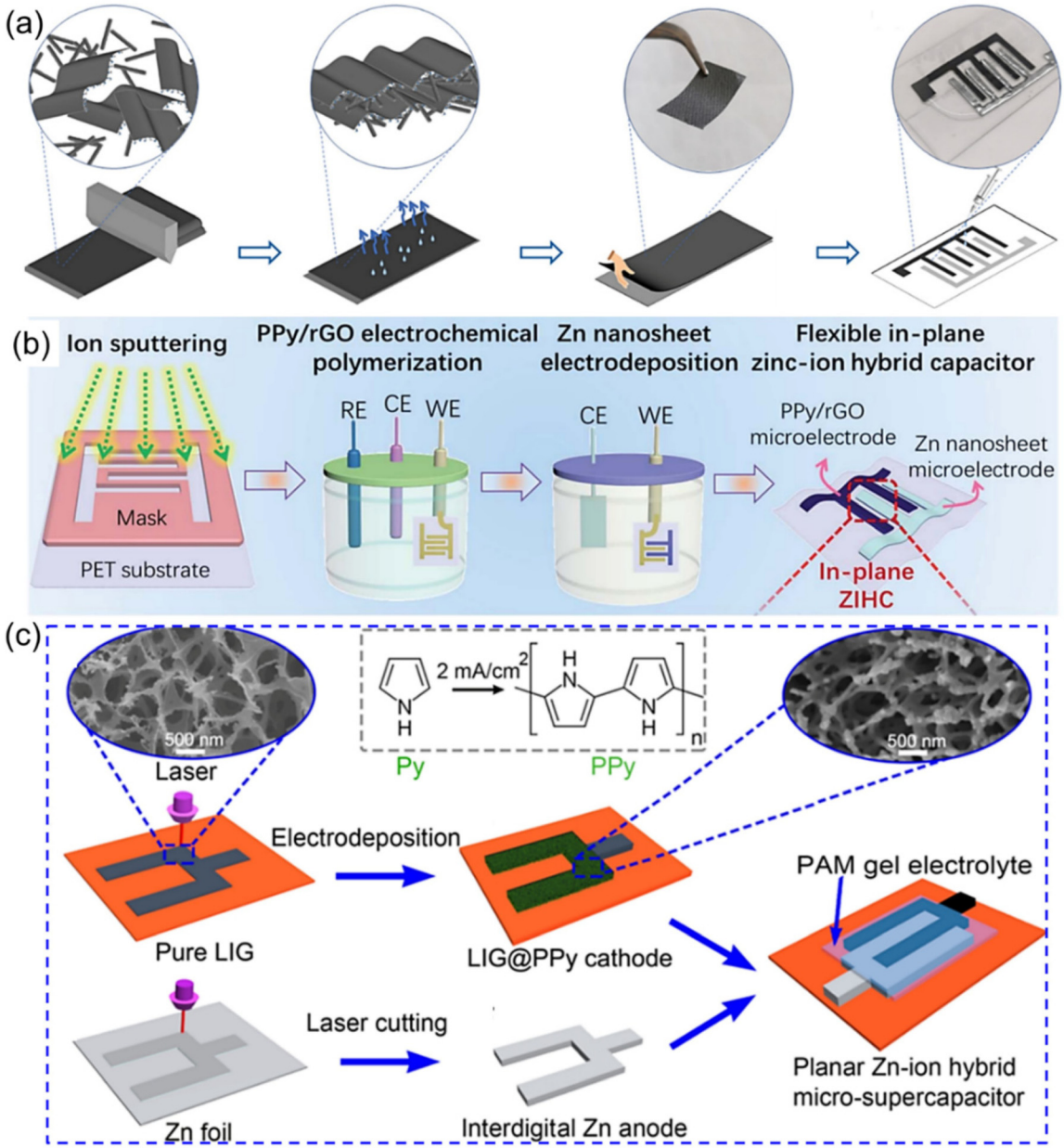


**Fig. 5** (a) Illustration of the fabrication of ZIHMSCs based on a graphene/PANI micro-cathode and Zn micro-anode. Reproduced with permission from ref. 98. Copyright 2023, MDPI. (b) Schematic diagram of the preparation process of the flexible in-plane PPY/rGO//Zn ZIHMSCs. Reproduced with permission from ref. 93. Copyright 2022, The Royal Society of Chemistry. (c) Schematic illustration of the preparation process of the ZIHMSC based on LIG@PPy micro-cathode and interdigitated Zn micro-anode. Reproduced with permission from ref. 99. Copyright 2022, American Chemical Society.

structural integrity of the porous structure to ensure fast charge diffusion kinetics.[99] As a result, the as-fabricated ZIHMSCs composed of LIG@PPy micro-cathode and Zn micro-anode exhibited a wide voltage window (1.7 V) and 200× enhancement in the areal capacitance/energy density as compared to that of the pristine LIG counterpart.[98] Very recently, it has been proved that fluorinated LIG (FLIG) with interconnected porous structure can not only serve as cathode material, but also act as an ideal substrate for the uniform electrodeposition of Zn nanosheets.[100] The as-obtained ZIHMSCs consisting of the FLIG cathode and Zn@FLIG anode delivered more than 15 times enhancement in both the areal capacitance (42.32 *vs.* 2.73 mF $cm^{-2}$) and energy density (15.1 *vs.* 0.97 μW h $cm^{-2}$) than the commercial LIG based ZHMSCs (42.32 *vs.* 2.73 mF $cm^{-2}$), respectively.

In addition to a large surface area, the microstructure and pore distribution of carbon-based cathode materials also play important roles in the overall performance of ZIHMSCs.[47,101] For example, flexible ZIHMSCs were constructed by a facile and economical in-plane asymmetric printing technology,

where a kelp-carbon cathode and Zn powder anode were screen printed onto Au current collectors (Fig. 6a), followed by coating the $Zn(CF_3SO_3)_2$-polyacrylamide (PAM) hydrogel electrolyte onto the interdigitated electrodes.[101] The unique 3D hierarchical architecture (Fig. 6b and c) of the kelp-carbon and multivalent ion storage mechanism enabled the printed quasi-solid-state ZIHMSCs with high areal capacitance (up to 10.3 mA h $cm^{-2}$) (Fig. 6d) and high areal energy density (up to

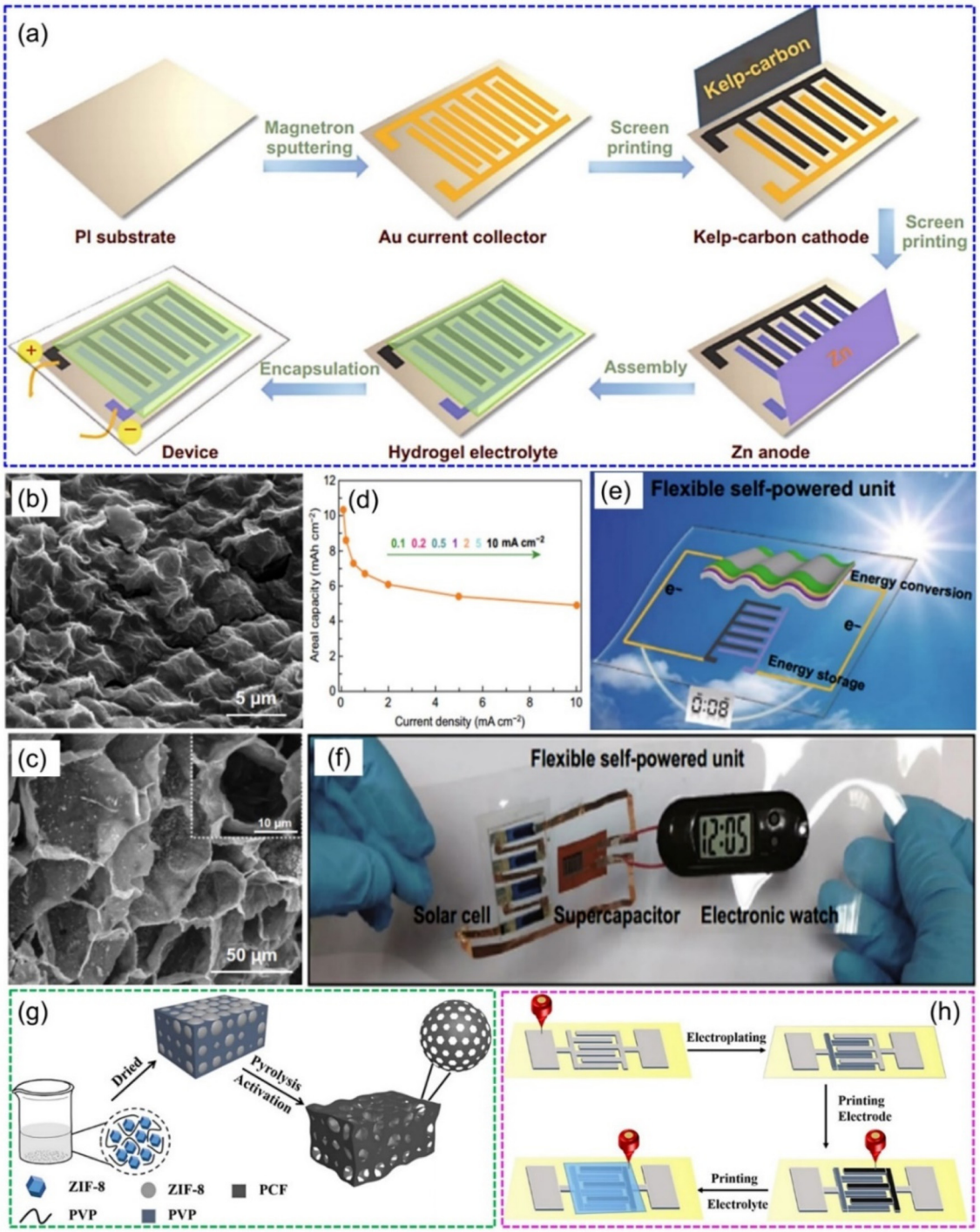


**Fig. 6** (a) Illustration of the fabrication process of flexible quasi-solid-state ZIHMSCs. SEM images of (b) surface and (c) interior morphologies of the kelp-carbon micro-cathode. (d) Rate capability of the as-prepared ZIHMCs. (e) Schematic illustration of the solar-charging self-powered unit. (f) Proof-of-concept demonstration of the flexible solar-charging self-powered unit. Reproduced with permission from ref. 101. Copyright 2020, Springer Nature. (g) Schematic illustration of the synthesis process of PCF. (h) Illustration of the fabrication process for the direct ink printed ZIHMSCs based on a PCF micro-cathode and Zn micro-anode. Reproduced with permission from ref. 102. Copyright 2021, WILEY-VCH.

 

8.2 μW h $cm^{-2}$), showing great promise for the design of energy integrated systems toward the goal of developing light weight and high-performance flexible electronics (Fig. 6e and f). Also, a flexible high-performance ZIHMSC was fabricated using ink direct printing of hierarchical honeycomb-like porous carbon frameworks (PCF) on stone paper as cathode (Fig. 6g and h).[102] Benefiting from its the hierarchically porous structure and outstanding conductivity of the PCF, the as-fabricated ZIHMSCs showed high specific capacity of 189.06 mA h $g^{-1}$ at a current density of 1 mA $cm^{-2}$ and superior durability (95.71% capacity retention at 10 mA $cm^{-2}$ after 1000 cycles).

### 4.2 MXene-based micro-cathodes

2D transition-metal carbides and nitrides (MXenes) as layered pseudocapacitive cathode materials possess typical features of excellent electrical conductivity, high specific capacitance, and remarkable flexibility, which are perfect for various high-performance energy storage systems.[103–105] Generally, MXene can be synthesized by etching out the layer A from $M_{n+1}AX_n$ phases ($n$ = 1, 2, or 3), where M refers to an early transition metal (*e.g.*, Ti, V, Cr, Mo, *etc.*) or multiple metals; A mainly represents a group IIIA or IVA element, and X is C and/or N.[104,105] By combining the advantages of the MXene cathode materials and novel microelectrode fabrication technology, MXene-based ZIHMSCs with superior electrochemical performance have been developed in the past five years. For instance, a flexible ZIHMSCs was fabricated using $Ti_3C_2T_x$ as the cathode by the laser direct writing method (Fig. 7a), followed by *in situ* annealing treatment.[95] The as-prepared ZIHMSCs exhibited excellent electrochemical performance with a high areal capacitance of 72.02 mF $cm^{-2}$ (at 10 mV $s^{-1}$), areal energy density of 0.02 mWh $cm^{-2}$ (at a power density of 0.50 mW $cm^{-2}$), and remarkable cycling stability (80% capacitance retention after 50 000 cycles), which indicated great potential for applications in the next-generation portable electronic devices. Moreover, in-plane Zn//$V_3CrC_3T_x$ MSCs was fabricated on paper, which displayed an ultra-high area energy-density of 51.12 mWh $cm^{-2}$, excellent cycling stability (84.5% capacitance retention after 20 000 cycles), and superior bendability (80.2% capacitance retention after 10 000 cycles).[106] These remarkable electrochemical performances of the obtained ZIHMSCs were attributed to the introduction of Cr into the $V_4C_3T_x$ lattice that can increase the adsorption sites of Zn ions, enable the MXene lattice to expand, and decrease the diffusion energy-barrier ($Zn^{2+}$), thus improving the specific capacitance and promoting the discharging potential and long-term cycling stability.

To enable the MXene micro-cathode based ZIHMSCs with enhanced electrochemical performance, another effective strategy is to adjust and modulate its interlayer spacing by intercalation of appropriate intercalators. With this in mind, Liu *et al.* delaminated 2D $Ti_3C_2T_x$ MXene cathodes using *N,N*-dimethylacetamide (DMAC), acetonitrile (ACN), LiCl ($H_2O$), and dimethyl sulfoxide (DMSO) (Fig. 7b), respectively, and found that DMAC intercalated $Ti_3C_2T_x$-based MSCs delivered a high volumetric capacitance of 1873 F $cm^{-3}$ (at 5 mV $s^{-1}$) (Fig. 7c), much higher than 1313 F $cm^{-3}$ for $Ti_3C_2T_x$-ACN, 1103 F $cm^{-3}$ for $Ti_3C_2T_x$–$H_2O$, and 544 F $cm^{-3}$ for $Ti_3C_2T_x$-DMSO, indicating that amide group-functionalized $Ti_3C_2T_x$ cathode based ZIHMSCs possess excellent electrochemical performance.[107] Notably, the $Ti_3C_2T_x$-DMAC cathode based ZIHMSCs showed superior flexibility and excellent cycling stability (invariable capacitance under 5000 bending cycles) (Fig. 7d), demonstrating their great potential in integrated wearable electronics. Additionally, a simple and scalable laser engraving process is demonstrated for the construction of multifunctional ZIHMSCs using the interlayer-spacing-regulated 3D MXene/rGO foam as the micro-cathode material (Fig. 7e).[108] Owing to the unique advantages of the 3D MXene/rGO foam such as controllable porosity and density, appropriate interlayer spacing, and good mechanical strength, the obtained ZIHMSCs displayed a large areal capacitance (83.96 mF $cm^{-2}$ at a current density of 0.5 mA $cm^{-2}$), low self-discharge rate (2.75 mV $h^{-1}$), and good cycling stability. Very recently, Cao *et al.* developed MXene/bacterial cellulose (BC) electrodes with fast ion transport channels by intercalating BC between MXene interlayers *via* interlayer transport channel engineering (Fig. 7f).[109] Owing to the fast anion intercalation/deintercalation of MXene/BC capacitor-type micro-cathode and reversible Zn stripping/plating on the Zn foil micro-anode (Fig. 7g), the as-fabricated ZIHMSCs showed a wider working voltage window (1.36 V), better cycling stability (70% after 10 000 cycles), and much higher areal capacitance than those of the ZIHMSCs based on the pure MXene cathode (404 *vs.* 239 mF $cm^{-2}$ at 1 mA $cm^{-2}$), demonstrating great potential for applications as the next-generation microscale power sources in small electronics (Fig. 7h).

## 5. Design and application of functional electrolytes

Electrolytes for ZIHMSCs are like blood for human beings, so electrolyte is an essential component of the ZIHMSCs. Importantly, the electrolyte plays a critical role, affecting the properties of the electrode/electrolyte interface and thus the electrochemical performance of the devices, such as electrochemical potential window, coulombic efficiency, cycle life, and safety.[110] In general, electrolytes can be classified into several categories including aqueous, organic, ionic liquid, and (quasi-) solid-state.[46,49] Ideally, electrolytes should possess a wide stable potential window, high ionic conductivity, good chemical stability, wide operating temperature range, low volatility and flammability, environment friendliness, and low cost.[111] However, each class of electrolyte possesses its own unique characteristics (Fig. 8a–c) and thus, trade-offs must be carefully managed, and the selection of an appropriate electrolyte is crucial to suit different forms of the ZIHMSCs.[46,49] Aqueous electrolytes are the most common electrolytes for the ZIHMSCs due to their advantages such as high ionic conductivity, non-flammability, low cost, and environment friendliness.[46,49,50] Among them, the neutral/mild acid electrolytes (*e.g.*, $ZnSO_4$, $Zn(CF_3SO_3)_2$) are preferable electrolytes than alkaline electrolytes, which is attributed

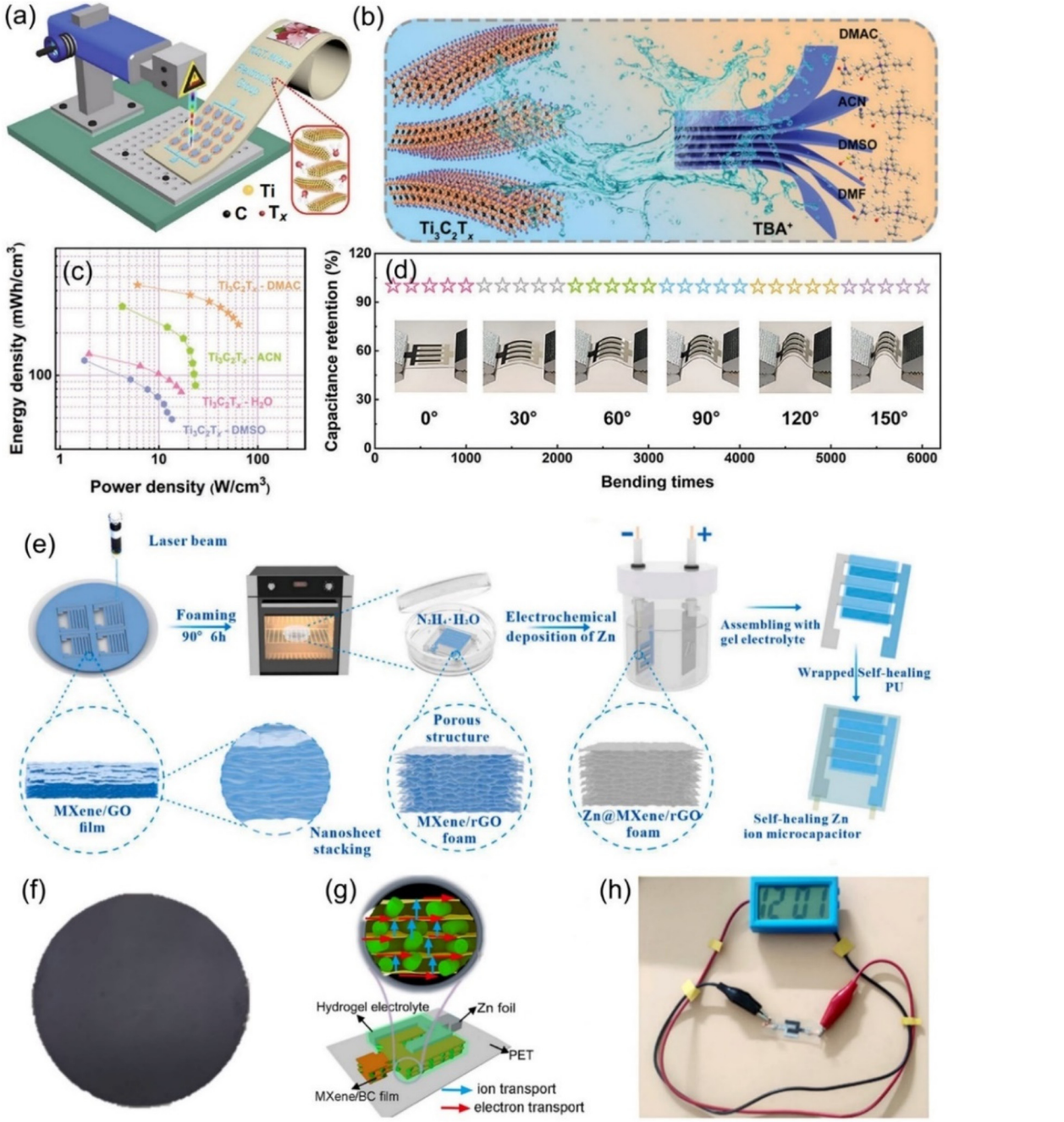


**Fig. 7** (a) Illustration of the fabrication process of the patterned MSCs array *via* laser writing technology. Reproduced with permission from ref. 95. Copyright 2021, Springer Nature. (b) Schematic diagram of the interaction process of different organic molecules. (c) Ragone plot of the corresponding ZIHMSCs. (d) Capacitance retention of the resulting ZIHMSCs under increased bending states. Reproduced with permission from ref. 107. Copyright 2022, WILEY-VCH. (e) Illustration of the assembly of ZIHMSCs based on a MXene/rGO foam micro-cathode and Zn micro-anode. Reproduced with permission from ref. 108. Copyright 2022, Elsevier. (f) Photograph of the as-prepared MXene/bacterial cellulose (BC)-3 : 2 film. (g) Schematic diagram of the assembled ZHMSCs and corresponding ion and electron transport. (h) Photograph of the obtained ZIHMSCs powering a small device. Reproduced with permission from ref. 109. Copyright 2023, WILEY-VCH.

to their outstanding stability and compatibility with the electrodes.[112] It is no doubt that they are also the first choice as the electrolytes of the ZIHMSCs. As a representative example, Wang *et al.* investigated the electrochemical performance of the ZIHMSCs in three different aqueous electrolytes: $ZnSO_4$, $ZnCl_2$, and $Zn(CF_3SO_3)_2$, respectively. Interestingly, the results not only demonstrated that the device displayed much better performance in $ZnSO_4$ electrolyte in terms of potential window and specific capacity, but also revealed that $SO_4^{2-}$ participated in the reaction.[92]

 

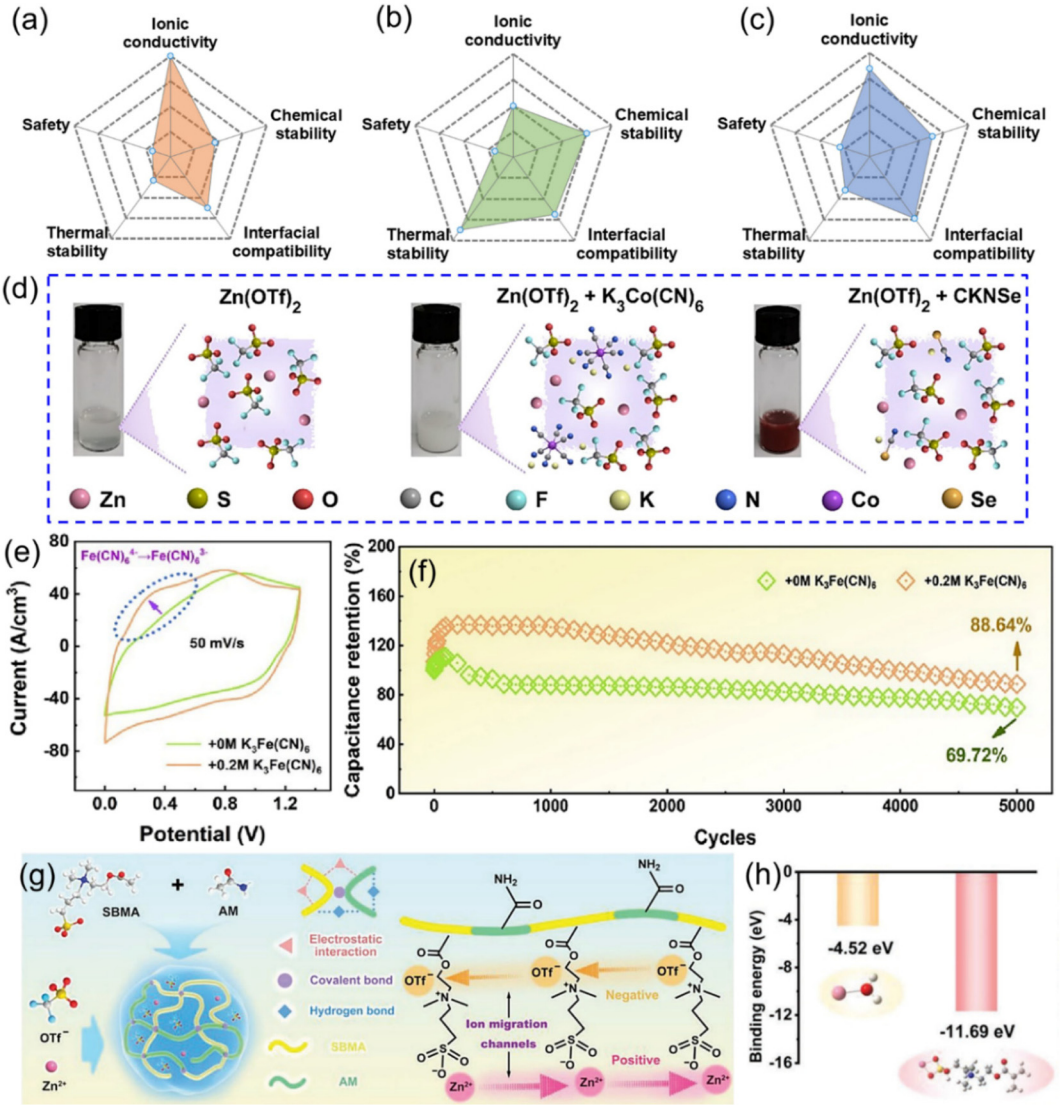


**Fig. 8** Radar maps showing the comparison of (a) aqueous electrolyte, (b) organic electrolyte, and (c) gel electrolyte, respectively. (d) Photos and molecular structures of the pure $Zn(OTf)_2$ electrolyte and hybrid electrolytes containing $K_3Co(CN)_6$ or CKNSe additives. Reproduced with permission from ref. 87. Copyright 2023, The Royal Society of Chemistry. (e) CV curves tested in $KFCN_0$ and $KFCN_{0.2}$ electrolytes. (f) Cycling stability of $Ti_3C_2T_x$-DMAC MXene-based ZIHMSCs separately tested in $KFCN_0$ and $KFCN_{0.2}$ electrolytes. Reproduced with permission from ref. 113. Copyright 2023, American Chemical Society. (g) Schematic diagram of fabrication, cross-linked structure, and ion migration channels of PASHE consisting of P(AM-*co*-SBMA) polymeric skeleton and $Zn(OTf)_2$ electrolyte. (h) Binding energies of $Zn^{2+}$–$H_2O$ and $Zn^{2+}$–PASHE based on simulation. Reproduced with permission from ref. 114. Copyright 2022, WILEY-VCH.

Additionally, incorporating redox-active additives into electrolytes is another common and effective approach for boosting the electrochemical performance. In general, the possible functions of electrolyte additives to improve electrochemical performance of the device are mainly based on the following aspects: (a) suppressing dendrite formation, (b) stabilizing electrode structure, and (c) providing additional capacity contribution.[87,115] Based on these advantages, Liu *et al.* separately investigated the effects of two different electrolyte additives on the electrochemical performance of ZIHMSCs (Fig. 8d). The results revealed that the ZIHMSCs with $K_3Co(CN)_6$ additive exhibited better rate capability and cycling stability than the device with potassium selenocyanate (CKNSe) additive and no additive. The enhanced performance was due to $K_3Co(CN)_6$ additive being able to introduce additional redox reaction ($Co^{2+} \leftrightarrow Co^{3+}$) during the charge/discharge processes, which was beneficial for improving the reversibility of Zn stripping/plating behaviors.[87] Following the same strategy, the same group further introduced $K_4Fe(CN)_6$ additive into $Zn(CF_3SO_3)_2$ gel electrolyte (Fig. 8e). It was noted that $K_4Fe(CN)_6$ additive can significantly improve rate performance, increase volumetric capacitance, and enhance cycling stability of the device (Fig. 8f). These excellent performances were attributed to the introduced redox reaction between $Fe^{2+}$ and $Fe^{3+}$, which

can obviously regulate the Zn stripping/plating behaviors and provide additional faradaic pseudocapacitance.[113]

Furthermore, motivated by the need to be integrated with miniaturized electronic platforms as well as satisfying the requirements of harsh conditions such as highly complex states (*e.g.*, pressing, twisting, stretching), the regular aqueous electrolytes may be not suitable for those new demands. This is because the commonly used aqueous electrolytes do not cover the patterned design entirely as it might cause short circuit failures especially when multiple devices are connected in tandem.[116] As such, gel-based electrolytes, which are usually prepared by mixing zinc salts (*e.g.*, $ZnSO_4$, $ZnCl_2$, $Zn(CF_3SO_3)_2$) with polymeric matrices (*e.g.*, polyvinyl alcohol, polyacrylamide) are prominent as they not only enable good electrode/electrolyte interface contact but also suppress the dendrite growth and reduce other side effects. Because the presence of hydrophilic groups in polymeric hydrogel electrolytes can reduce $H_2O$ activity, they also effectively reduce the side reactions (*e.g.*, corrosion, $H_2$ evolution). However, slow $Zn^{2+}$ ion transport and desolvation of hydrated $Zn^{2+}$ in the hydrogel electrolyte attenuated the expected effect of suppressing dendrites and parasitic reactions. To alleviate such issues, a zwitterionic hydrogel electrolyte containing a pair of oppositely charged groups was designed and synthesized.[114] Acrylamide (AM) and [2-(methacryloyloxy)ethyl] dimethyl-(3-sulfopropyl) (SBMA) monomers were co-polymerized and subsequently immersed in $Zn(OTf)_2$ solution to form a zwitterionic P(AM-*co*-SBMA) hydrogel electrolyte (PASHE) (Fig. 8g). The zwitterionic groups within the hydrogel created ion migration channels that promoted the transportation of the $Zn^{2+}$ ions. Moreover, the strongly polar sulfobetaine sulfonate anion of the polymeric matrix in PASHE possessed much stronger adsorption of $Zn^{2+}$ as evidenced by the much lower binding energy (Fig. 8h). Hence, this led to enhanced desolvation of hydrated $Zn^{2+}$ and accelerated the Zn plating/stripping kinetics.

## 6. Applications of ZIHMSCs

ZIHMSCs have unique merits such as small size, light weight, and long cycling durability making them promising power

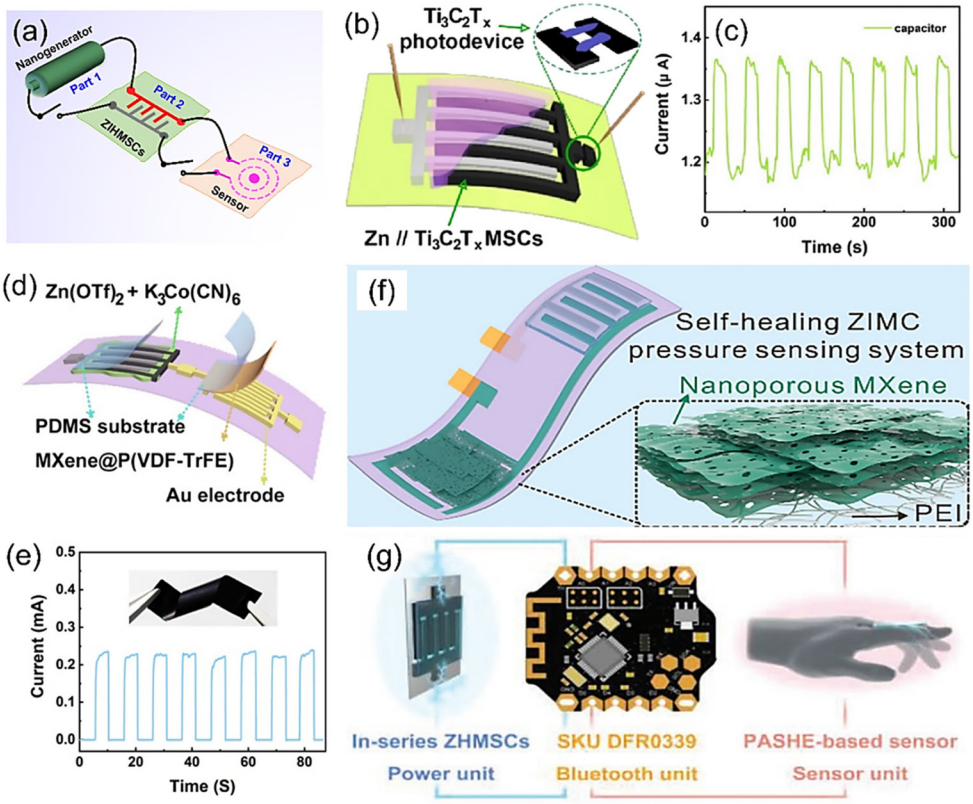


**Fig. 9** (a) Illustration of the integrated self-power system. (b) Schematic diagram of the $Ti_3C_2T_x$ MXene-based ZIHMSC-photodetector system and (c) its corresponding current response curves. Reproduced with permission from ref. 113. Copyright 2023, American Chemical Society. (d) Integrated unit constructed from $Ti_3C_2T_x$-DMSO MXene-based ZIHMSCs and $Ti_3C_2T_x$-DMF@P(VDF–TrFE)-based pressure sensor, and (e) its corresponding current response under compression and release conditions. Inset in (e) is the obtained $Ti_3C_2T_x$-DMF@P(VDF–TrFE) film. Reproduced with permission from ref. 87. Copyright 2023, The Royal Society of Chemistry. (f) Schematic diagram of integrated system constructed from a ZIHMSCs and a nanoporous $Ti_3C_2T_x$ MXene-based pressure sensor. Reproduced with permission from ref. 117. Copyright 2022, Elsevier. (g) Schematic of the integrated unit consisting of an electrolyte (PASHE)-based sensor, Bluetooth system, and ZIHMSCs. Reproduced with permission from ref. 114. Copyright 2022, WILEY-VCH.

 

**Table 1** Electrochemical performance comparison of some representative ZIHMSCs

| Zn micro-anode | | Micro-cathode | | | | | | |
|---|---|---|---|---|---|---|---|---|
| Materials | Preparation methods | Materials | Preparation methods | Electrolyte | Potential (V) | Areal capacitance (mF $cm^{-2}$) | Energy density (μWh $cm^{-2}$) | Capacitance retention/cycles | Ref. |
| Zn film | Cyclic voltammetry | CNTs | Laser engraving | $ZnSO_4$ gel | 0–1.8 | 83.2 (1 mA $cm^{-2}$) | 29.6 | 87.4%/6000 | 1 |
| Zn film | Potentiostatic deposition | AC | Injection | $ZnSO_4$ | 0.5–1.5 | 1297 (0.16 mA $cm^{-2}$) | 115.4 | 100%/10 000 | 27 |
| Zn foil | Laser writing | AC | Brush coating | Gelatin/$ZnSO_4$ gel | 0–1.8 | 605 (0.2 mA $cm^{-2}$) | 215.1 | 68%/500 | 83 |
| Zn powder | Spray coating | $Ti_3C_2T_x$-DMSO | Spray coating | $K_3Co(CN)_6$/Zn$(CF_3SO_3)_2$/PVA | 0–1.3 | 759.4 F $cm^{-3}$ (20 mV $s^{-1}$) | 178.3 μWh $cm^{-3}$ | 70%/5000 | 87 |
| Zn film | Potentiostatic deposition | Poly(3,3′-DHB)/AC | Electrochemical polymerization | $ZnSO_4$ gel | −0.15–0.85 | 1100 (0.5 mA $cm^{-2}$) | 152 | 80%/3000 | 92 |
| Zn film | Galvanostatic deposition | PPy/rGO | Electrochemical polymerization | Zn$(CF_3SO_3)_2$/PVA | 0–1.6 | 92.5 (0.2 mA $cm^{-2}$) | 25.2 | 92%/10 000 | 93 |
| Zn film | Potentiostatic deposition | $Ti_3C_2T_x$ | Laser cutting | $ZnCl_2$/PVA | 0–1.5 | 72.02 (10 mV $s^{-1}$) | N.A. | 80%/50 000 | 95 |
| Zn foil | Laser cutting | EG/PANI film | Laser cutting | PVA/$ZnCl_2$ gel | 0–0.6 | 1800 (2.6 mA $cm^{-2}$) | 755.8 | 88.7%/2000 | 98 |
| Zn foil | Laser cutting | LIG@PPy | Electrochemical polymerization | $ZnSO_4$/PAM gel | 0–1.7 | 149 (0.31 mA $cm^{-2}$) | 54 | 79%/2000 | 99 |
| Zn@FLIG | Potentiostatic deposition | FLIG | Laser engraving | PVA/$ZnCl_2$ gel | 0.2–1.8 | 42.32 (0.1 mA $cm^{-2}$) | 15.1 | 79.4%/7000 | 100 |
| Zn powder | Screen printing | Kelp-carbon | Screen printing | Zn$(CF_3SO_3)_2$/PAM gel | 0.1–1.7 | 10.3 μA h $cm^{-2}$ (0.1 mA $cm^{-2}$) | 8.2 | 95%/100 | 101 |
| Zn film | Galvanostatic deposition | PCF | Ink printing | $ZnSO_4$ gel | 0.2–1.8 | 189.06 mA h $g^{-1}$ (1 mA $cm^{-2}$) | 76.38 Wh $kg^{-1}$ | 95.7%/1000 | 102 |
| Zn | Galvanostatic deposition | $V_3CrC_3T_x$ MXene | Screen printing | $ZnSO_4$/PVA | 0–1.3 | 1680.2 (5 mg $cm^{-2}$) | 51.12 | 84.5%/20 000 | 106 |
| Zn powder | Spray coating | $Ti_3C_2T_x$-DMAC | Spray coating | Zn$(CF_3SO_3)_2$/PVA | 0–1.3 | 52 (5 mV $s^{-1}$) | 12.09 | 70%/5000 | 107 |
| Zn-MXene/rGO film | Potentiostatic deposition | 3D MXene/rGO | Laser cutting | Gelatin/$ZnSO_4$ gel | 0–1.4 | 83.96 (0.5 mA $cm^{-2}$) | 10.1 | 80.8%/1400 | 108 |
| Zn foil | N.A. | MXene/BC | N.A. | Zn$(CF_3SO_3)_2$/PAM gel | 0–1.36 | 404 (1 mA $cm^{-2}$) | 94 | 70%/10 000 | 109 |
| Zn powder | Spray coating | $Ti_3C_2T_x$-DMAC | Spray coating | $K_3Fe(CN)_6$/Zn$(CF_3SO_3)_2$/PVA | 0–1.3 | 2107.4 F $cm^{-3}$ (5 mV $s^{-1}$) | 494.7 mWh $cm^{-3}$ | 88.6%/5000 | 113 |
| Zn powder | Mask-assisted deposition | AC | Mask-assisted deposition | PASHE | 0.2–1.8 | 76.3 (2 mA $cm^{-2}$) | N.A. | 94.6%/17 000 | 114 |

source candidates. As mentioned previously, ZIHMSCs have shown practical applications in powering small devices such as LED lights and stopwatches. To further expand their potential applications into new advanced complex systems, ZIHMSCs have been integrated with other functional electronic devices to design self-power integrated systems (Fig. 9a). In this section, several representative applications of the ZIHMSCs in microelectronic systems are briefly summarized. As a conceptual demonstration of an integrated system, a $Ti_3C_2T_x$ MXene-based ZIHMSCs-photodetector system was constructed by the *in situ* integration of the photodetector beside the $Ti_3C_2T_x$ MXene-based ZIHMSCs (Fig. 9b),[113] where the $Ti_3C_2T_x$ MXene cathode electrode acts as one electrode of the photodetector. The time-dependent photo-response of the photodetector driven by the $Ti_3C_2T_x$ MXene-based ZIHMSCs was evaluated by periodically turning the laser on/off. The on/off ratio of the photocurrent was 1.13 (Fig. 9c), indicating the good stability of the $Ti_3C_2T_x$ MXene-based ZIHMSC-photodetector unit. In addition to the ZIHMSC-photodetector system, the ZIHMSC-pressure sensor system has also attracted much attention because it can be used to monitor the health status of the human body under different activities. As an example, a flexible ZIHMSC-pressure sensor integrated unit was constructed using $Ti_3C_2T_x$-DMSO MXene-based ZIHMSCs and a MXene@P(VDF-TrFE) pressure sensor (Fig. 9d). Note that the pressure sensor powered by the ZIHMSCs can generate a relatively large current response during compression and release cycles (Fig. 9e).[87] As another representative example, a ZIHMSC-pressure sensor system was constructed from a ZIHMSC and a nanoporous $Ti_3C_2T_x$ MXene-based pressure sensor (Fig. 9f),[117] in which a layered porous-MXene membrane and an electrospun PEI served as the pressure sensing part and isolation part, respectively. Encouragingly, with the power provided by the ZIHMSCs, the pressure sensing system works well under different human activities and can be used to monitor the health status. In addition, Zhang *et al.* introduced a very interesting integrated unit consisting of a polymer electrolyte (PASHE)-based sensor, a Bluetooth system, and ZIHMSCs (Fig. 9g). In particular, PASHE can be directly used as a sensor due to its excellent ionic conductivity. Surprisingly, the obtained integrated device can be employed to monitor the finger movements based on resistance changes.[114] It should be mentioned that these encouraging works are still in the lab-scale, and their applications in self-powered systems are still in infancy. To further demonstrate the potential applications of ZIHMSCs in the integrated wearable/portable electronic devices, it is highly desirable to explore new ZIHMSCs with compatible structures and remarkable performance to power other sensors (*e.g.*, gas sensor, temperature sensor, humidity sensor), thereby designing and

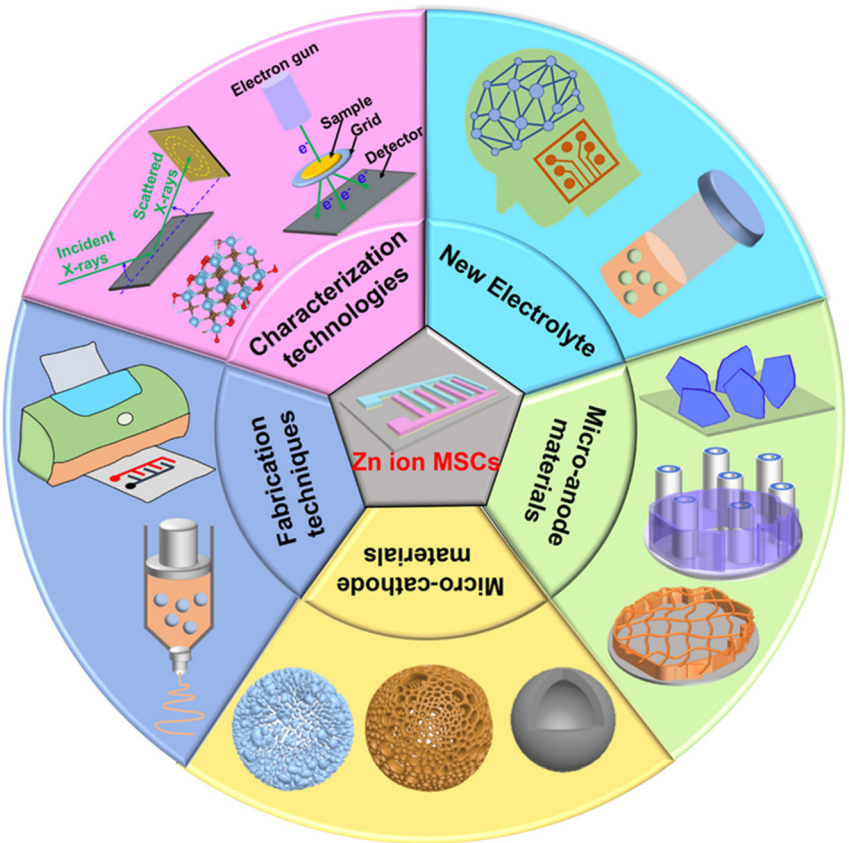


Fig. 10 Special attention and future directions on different aspects and components for the construction of high-performance ZIHMSCs.

 

constructing new integrated self-powered systems with multiple functions and high safety.

## 7. Challenges and perspectives

In summary, we reviewed the state-of-the-art advances of ZIHMSCs (Table 1), with an emphasis on the design and construction of Zn micro-anodes and advanced micro-cathodes with unique morphologies and structures using different strategies, the development of novel and compatible electrolyte systems, and fundamental understanding of their effects on device performance as well as energy storage mechanisms. Although great achievements have been made during the past few years, there are still lots of challenging issues that need to be addressed before the large-scale applications of the ZIHMSCs, such as the lack of high-performance micro-cathodes, highly stable Zn micro-anodes, and suitable electrolyte systems. Therefore, proper control of the composition, morphology, and structure of the cathode and anode micro-electrodes along with suitable electrolyte systems are crucial factors to pursue high-performance ZIHMSCs. From our perspective, future attention on ZIHMSCs including challenges and technical problems should be directed towards the following aspects (Fig. 10).

(a) Design and construction of advanced Zn micro-anodes with high reversibility and long-term durability. Despite the abovementioned achievements, several practical aspects still need to be considered, such as current density and deposited/stripped capacity, both of which can significantly affect the electrochemical behavior of the Zn micro-anodes. Furthermore, special attention towards improving the high reversibility and long-term durability of the Zn micro-anodes is also of great significance to meet the needs of large-scale energy storage applications.

(b) Using different strategies to explore novel micro-cathode materials with high capacity and excellent stability. As reported, the capacity of most present cathodes cannot match well the capacity of the metallic zinc anode. Based on the "wooden barrel theory", the energy density of the ZIHMSCs is obviously limited by the low specific capacity of micro-cathodes. In this scenario, future research can focus on developing novel high-performance micro-cathode materials through effective engineering strategies, thus ensuring electrical conductivity, fast ion diffusion kinetics, and long-term durability.

(c) Design and development of novel suitable electrolyte systems. As an important component of ZIHMSCs, electrolytes play an important role in influencing the electrochemical performance of the device. So far, several different types of electrolytes have been developed, but their properties and performance remain unsatisfactory because each type has its own drawbacks and benefits. For example, most reported neutral/mild acid electrolytes still suffer from unsatisfactory zinc stripping/plating coulombic efficiency and narrow electrochemical stable potential windows. Therefore, there is an urgent need to develop novel electrolyte systems and/or explore the new concept of "beyond aqueous" electrolytes with low-cost, easy-processing, high ionic conductivity, and wide operating voltage. Additionally, the selection and optimization of suitable electrolytes still rely on inefficient trial-and-error procedures, so it would be an interesting endeavor to design and synthesize promising electrolyte candidates with the assistance of machine learning and artificial intelligence.

(d) Using advanced techniques and combining theoretical simulations to investigate the energy storage mechanism. As mentioned before, the energy storage mechanism of ZIHMSCs remains unclear and controversial, which is closely related to the electrode materials and electrolytes used. In this case, it is necessary to adopt comprehensive electrochemical methods, advanced *ex situ* and *in situ* characterization techniques and theoretical calculations to understand the energy storage mechanisms of the electrode materials in different kinds of electrolyte systems. This will provide guidance and reference for other researchers.

(e) Developing new, easy-processing, and scalable techniques for the construction of high-performance ZIHMSCs. Although various approaches have been employed to design and prepare ZIHMSCs, these reported fabrication techniques are still far from satisfactory for large-scale applications because of some drawbacks, such as complex procedures, time consumption, and high cost. Therefore, particular emphasis should be given to explore cost-effective, easy processing, and scalable fabrication techniques.

## Conflicts of interest

There are no conflicts of interest to declare.

## References

1 G. Sun, H. Yang, G. Zhang, J. Gao, X. Jin, Y. Zhao, L. Jiang and L. Qu, *Energy Environ. Sci.*, 2018, **11**, 3367–3374.
2 G. H. An, J. Hong, S. Pak, Y. Cho, S. Lee, B. Hou and S. Cha, *Adv. Energy Mater.*, 2019, **10**, 1902981.
3 M. Yu, Y. Peng, X. Wang and F. Ran, *Adv. Funct. Mater.*, 2023, **33**, 2301877.
4 W. Zong, Y. Ouyang, Y. E. Miao, T. Liu and F. Lai, *Chem. Commun.*, 2022, **58**, 2075–2095.
5 H. Liu, Z. Sun, Y. Chen, W. Zhang, X. Chen and C. P. Wong, *ACS Nano*, 2022, **16**, 10088–10129.
6 J. Zhang, G. Zhang, T. Zhou and S. Sun, *Adv. Funct. Mater.*, 2020, **30**, 1910000.
7 N. A. Kyerematen, T. Brousse and D. Pech, *Nat. Nanotechnol.*, 2017, **12**, 7–15.
8 D. Wang, C. Han, F. Mo, Q. Yang, Y. Zhao, Q. Li, G. Liang, B. Dong and C. Zhi, *Energy Storage Mater.*, 2020, **28**, 264–292.
9 X. Wang and Z. S. Wu, *EcoMat*, 2020, **2**, e12042.
10 X. Shi, P. Das and Z.-S. Wu, *ACS Energy Lett.*, 2021, **7**, 267–281.

11 C. Lethien, J. Le Bideau and T. Brousse, *Energy Environ. Sci.*, 2019, **12**, 96–115.
12 Z. Zhu, R. Kan, S. Hu, L. He, X. Hong, H. Tang and W. Luo, *Small*, 2020, **16**, e2003251.
13 C. Meng, J. Maeng, S. W. M. John and P. P. Irazoqui, *Adv. Energy Mater.*, 2013, **4**, 1301269.
14 A. Tyagi, K. M. Tripathi and R. K. Gupta, *J. Mater. Chem. A*, 2015, **3**, 22507–22541.
15 J. Jin, X. Geng, Q. Chen and T. L. Ren, *Nanomicro Lett.*, 2022, **14**, 64.
16 P. Dai, W. Zhang, T. Jiang, Y. Xiong and W. Mingzai, *APL Mater.*, 2023, **11**, 060601.
17 D. B. Basha, S. Ahmed, A. Ahmed and M. A. Gondal, *J. Energy Storage*, 2023, **60**, 106581.
18 Y. Zhu, S. Wang, J. Ma, P. Das, S. Zheng and Z.-S. Wu, *Energy Storage Mater.*, 2022, **51**, 500–526.
19 Y. Wu, B. Ma, S. Cheng, Y. Liu, S. Chen, J. Fu and E. Xie, *Electrochim. Acta*, 2022, **427**, 140864.
20 P. Zhang, F. Wang, S. Yang, G. Wang, M. Yu and X. Feng, *Energy Storage Mater.*, 2020, **28**, 160–187.
21 S. Zheng, X. Shi, P. Das, Z. S. Wu and X. Bao, *Adv. Mater.*, 2019, **31**, e1900583.
22 P. Zhang, S. Yang, H. Xie, Y. Li, F. Wang, M. Gao, K. Guo, R. Wang and X. Lu, *ACS Nano*, 2022, **16**, 17593–17612.
23 S. Bi, H. Cao, R. Wang, F. Wan and Z. Niu, *J. Energy Chem.*, 2021, **63**, 25–39.
24 T. S. D. Le, Y. A. Lee, H. K. Nam, K. Y. Jang, D. Yang, B. Kim, K. Yim, S. W. Kim, H. Yoon and Y. J. Kim, *Adv. Funct. Mater.*, 2021, **32**, 2107768.
25 Q. Xia, W. Zeng, F. Ji, X. Chen, Y. Zhang, F. Ling, W. Hu, L. Fang, S. N. Khisro and M. Zhou, *J. Mater. Chem. C*, 2019, **7**, 11441–11448.
26 H. Liu, K.-S. Moon, J. Li, Y. Xie, J. Liu, Z. Sun, L. Lu, Y. Tang and C.-P. Wong, *Nano Energy*, 2020, **77**, 105058.
27 P. Zhang, Y. Li, G. Wang, F. Wang, S. Yang, F. Zhu, X. Zhuang, O. G. Schmidt and X. Feng, *Adv. Mater.*, 2019, **31**, 1806005.
28 D. P. Dubal, D. Aradilla, G. Bidan, P. Gentile, T. J. S. Schubert, J. Wimberg, S. Sadki and P. Gomez-Romero, *Sci. Rep.*, 2015, **5**, 9771.
29 Y. He, P. Zhang, M. Wang, F. Wang, D. Tan, Y. Li, X. Zhuang, F. Zhang and X. Feng, *Mater. Horiz.*, 2019, **6**, 1041–1049.
30 J. Li, Y. Shao, C. Hou, Q. Zhang, Y. Li and H. Wang, *J. Mater. Chem. A*, 2020, **8**, 22083–22089.
31 S. Zheng, J. Ma, K. Fang, S. Li, J. Qin, Y. Li, J. Wang, L. Zhang, F. Zhou, F. Liu, K. Wang and Z. S. Wu, *Adv. Energy Mater.*, 2021, **11**, 2003835.
32 H. Wang, M. Wang and Y. Tang, *Energy Storage Mater.*, 2018, **13**, 1–7.
33 Y. Wu, M. Wu, D. Ho and H. Hu, *ACS Appl. Mater. Interfaces*, 2022, **14**, 55770–55779.
34 A. Li, Z. Wei, Y. Wang, Y. Zhang, M. Wang, H. Zhang, Y. Ma, C. Liu, J. Zou, B. Ge, F. Cheng and Y. Yue, *Chem. Eng. J.*, 2023, **457**, 141339.
35 W. Chen, Y. Zhou, M. Cao, Z. Shi, Y. Liu, C. Zhang, X. Li and Y. Ma, *J. Alloys Compd.*, 2023, **965**, 171488.
36 K. Mao, J. Shi, Q. Zhang, Y. Hou, L. Wen, Z. Liu, F. Long, K. Niu, N. Liu, F. Long and Y. Gao, *Nano Energy*, 2022, **103**, 107791.
37 Y. Wang, T. Yun, X. Wang, B. Yao, Z. Ye and X. Peng, *Mater. Today Energy*, 2023, **36**, 101359.
38 T. Huang, B. Gao, S. Zhao, H. Zhang, X. Li, X. Luo, M. Cao, C. Zhang, S. Luo, Y. Yue, Y. Ma and Y. Gao, *Nano Energy*, 2023, **111**, 108383.
39 P. Zhang, F. Wang, M. Yu, X. Zhuang and X. Feng, *Chem. Soc. Rev.*, 2018, **47**, 7426–7451.
40 T. Zhao, G. Zhang, F. Zhou, S. Zhang and C. Deng, *Small*, 2018, **14**, 1802320.
41 A. M. Gaikwad, G. L. Whiting, D. A. Steingart and A. C. Arias, *Adv. Mater.*, 2011, **23**, 3251–3255.
42 H. Liu, Y. Xie, J. Liu, K.-s. Moon, L. Lu, Z. Lin, W. Yuan, C. Shen, X. Zang, L. Lin, Y. Tang and C.-P. Wong, *Chem. Eng. J.*, 2020, **393**, 124672.
43 H. Hu, K. Zhang, S. Li, S. Ji and C. Ye, *J. Mater. Chem. A*, 2014, **2**, 20916–20922.
44 F. Wang, O. Borodin, T. Gao, X. Fan, W. Sun, F. Han, A. Faraone, J. A. Dura, K. Xu and C. Wang, *Nat. Mater.*, 2018, **17**, 543–549.
45 C. Xu, B. Li, H. Du and F. Kang, *Angew. Chem., Int. Ed.*, 2012, **51**, 933–935.
46 S. Gao, Z. Zhang, F. Mao, P. Liu and Z. Zhou, *Mater. Chem. Front.*, 2023, **7**, 3232–3258.
47 L. Dong, W. Yang, W. Yang, Y. Li, W. Wu and G. Wang, *J. Mater. Chem. A*, 2019, **7**, 13810–13832.
48 F. Yu, L. Pang, X. Wang, E. R. Waclawik, F. Wang, K. Ostrikov and H. Wang, *Energy Storage Mater.*, 2019, **19**, 56–61.
49 Y. Lv, Y. Xiao, L. Ma, C. Zhi and S. Chen, *Adv. Mater.*, 2022, **34**, 2106409.
50 C. Liu, X. Xie, B. Lu, J. Zhou and S. Liang, *ACS Energy Lett.*, 2021, **6**, 1015–1033.
51 S. D. Han, N. N. Rajput, X. Qu, B. Pan, M. He, M. S. Ferrandon, C. Liao, K. A. Persson and A. K. Burrell, *ACS Appl. Mater. Interfaces*, 2016, **8**, 3021–3031.
52 P. Liu, W. Liu, Y. Huang, P. Li, J. Yan and K. Liu, *Energy Storage Mater.*, 2020, **25**, 858–865.
53 C. Wang, X. Zeng, P. J. Cullen and Z. Pei, *J. Mater. Chem. A*, 2021, **9**, 19054–19082.
54 X. Gong, J. Chen and P. S. Lee, *Batteries Supercaps*, 2021, **4**, 1529–1546.
55 L. Dong, X. Ma, Y. Li, L. Zhao, W. Liu, J. Cheng, C. Xu, B. Li, Q.-H. Yang and F. Kang, *Energy Storage Mater.*, 2018, **13**, 96–102.
56 H. Zhang, Q. Liu, Y. Fang, C. Teng, X. Liu, P. Fang, Y. Tong and X. Lu, *Adv. Mater.*, 2019, **31**, 1904948.
57 Y. Zheng, W. Zhao, D. Jia, Y. Liu, L. Cui, D. Wei, R. Zheng and J. Liu, *Chem. Eng. J.*, 2020, **387**, 124161.
58 M. S. Javed, S. Asim, T. Najam, M. Khalid, I. Hussain, A. Ahmad, M. A. Assiri and W. Han, *Carbon Energy*, 2022, **5**, e271.

 

59 P. Hu, T. Zhu, X. Wang, X. Wei, M. Yan, J. Li, W. Luo, W. Yang, W. Zhang, L. Zhou, Z. Zhou and L. Mai, *Nano Lett.*, 2018, **18**, 1758–1763.
60 H. Pan, Y. Shao, P. Yan, Y. Cheng, K. S. Han, Z. Nie, C. Wang, J. Yang, X. Li, P. Bhattacharya, K. T. Mueller and J. Liu, *Nat. Energy*, 2016, **1**, 16039.
61 H. Wang, W. Ye, Y. Yang, Y. Zhong and Y. Hu, *Nano Energy*, 2021, **85**, 105942.
62 X. Deng, J. Li, Z. Shan, J. Sha, L. Ma and N. Zhao, *J. Mater. Chem. A*, 2020, **8**, 11617–11625.
63 S. Li, J. Chen, X. Gong, J. Wang and P. S. Lee, *Small*, 2018, **14**, 1804035.
64 K. Zhu, T. Wu and K. Huang, *Energy Storage Mater.*, 2021, **38**, 473–481.
65 F. Wang, E. Hu, W. Sun, T. Gao, X. Ji, X. Fan, F. Han, X.-Q. Yang, K. Xu and C. Wang, *Energy Environ. Sci.*, 2018, **11**, 3168–3175.
66 Y. Dong, S. Di, F. Zhang, X. Bian, Y. Wang, J. Xu, L. Wang, F. Cheng and N. Zhang, *J. Mater. Chem. A*, 2020, **8**, 3252–3261.
67 J. Yan, E. H. Ang, Y. Yang, Y. Zhang, M. Ye, W. Du and C. C. Li, *Adv. Funct. Mater.*, 2021, **31**, 2010213.
68 Z. Yi, G. Chen, F. Hou, L. Wang and J. Liang, *Adv. Energy Mater.*, 2020, **11**, 2003065.
69 W. Du, J. Yan, C. Cao and C. C. Li, *Energy Storage Mater.*, 2022, **52**, 329–354.
70 W. Guo, Z. Cong, Z. Guo, C. Chang, X. Liang, Y. Liu, W. Hu and X. Pu, *Energy Storage Mater.*, 2020, **30**, 104–112.
71 H. Yang, Z. Chang, Y. Qiao, H. Deng, X. Mu, P. He and H. Zhou, *Angew. Chem., Int. Ed.*, 2020, **59**, 9377–9381.
72 J. Shin, J. Lee, Y. Park and J. W. Choi, *Chem. Sci.*, 2020, **11**, 2028–2044.
73 L. Yuan, J. Hao, C.-C. Kao, C. Wu, H.-K. Liu, S.-X. Dou and S.-Z. Qiao, *Energy Environ. Sci.*, 2021, **14**, 5669–5689.
74 X. Guo and G. He, *J. Mater. Chem. A*, 2023, **11**, 11987–12001.
75 Y. Yu, J. Xie, H. Zhang, R. Qin, X. Liu and X. Lu, *Small Sci.*, 2021, **1**, 2000066.
76 J. Hao, X. Li, X. Zeng, D. Li, J. Mao and Z. Guo, *Energy Environ. Sci.*, 2020, **13**, 3917–3949.
77 Z. Zhou, Z. Pei, L. Wei, S. Zhao, X. Jian and Y. Chen, *Energy Environ. Sci.*, 2020, **13**, 3185–3206.
78 Z. Ye, Z. Cao, M. O. Lam Chee, P. Dong, P. M. Ajayan, J. Shen and M. Ye, *Energy Storage Mater.*, 2020, **32**, 290–305.
79 T. Wang, J. Sun, Y. Hua, B. N. V. Krishna, Q. Xi, W. Ai and J. S. Yu, *Energy Storage Mater.*, 2022, **53**, 273–304.
80 Q. Zhang, J. Luan, Y. Tang, X. Ji and H. Wang, *Angew. Chem., Int. Ed.*, 2020, **59**, 13180–13191.
81 N. Chaba, S. Neramittagapong, A. Neramittagapong and N. Eua-Anant, *Heliyon*, 2019, **5**, e02681.
82 L. Ma, N. Li, C. Long, B. Dong, D. Fang, Z. Liu, Y. Zhao, X. Li, J. Fan, S. Chen, S. Zhang and C. Zhi, *Adv. Funct. Mater.*, 2019, **29**, 1906142.
83 K. Chen, L. Yan, Y. Sheng, Y. Ma, L. Qu and Y. Zhao, *ACS Nano*, 2022, **16**, 15261–15272.
84 X. Zhao, Y. Gao, Q. Cao, F. Bu, J. Pu, Y. Wang and C. Guan, *Adv. Energy Mater.*, 2023, **13**, 2301741.
85 Q. Li, Y. Wang, F. Mo, D. Wang, G. Liang, Y. Zhao, Q. Yang, Z. Huang and C. Zhi, *Adv. Energy Mater.*, 2021, **11**, 2003931.
86 W. Du, S. Huang, Y. Zhang, M. Ye and C. C. Li, *Energy Storage Mater.*, 2022, **45**, 465–473.
87 W. Liu, L. Li and G. Shen, *Nanoscale*, 2023, **15**, 2624–2632.
88 X. L. Li and H. Y. Yang, *Mater. Today: Proc.*, 2022, **70**, 279–282.
89 Y. Lu, Z. Wang, M. Li, Z. Li, X. Hu, Q. Xu, Y. Wang, H. Liu and Y. Wang, *Adv. Funct. Mater.*, 2023, DOI: **10.1002/adfm.202310966**.
90 X. Wang, S. Zheng, F. Zhou, J. Qin, X. Shi, S. Wang, C. Sun, X. Bao and Z.-S. Wu, *Natl. Sci. Rev.*, 2020, **7**, 64–72.
91 Z. Kang, C. Wu, L. Dong, W. Liu, J. Mou, J. Zhang, Z. Chang, B. Jiang, G. Wang, F. Kang and C. Xu, *ACS Sustainable Chem. Eng.*, 2019, **7**, 3364–3371.
92 N. Wang, T. Xin, Y. Zhao, Q. Li, M. Hu and J. Liu, *ACS Sustainable Chem. Eng.*, 2019, **7**, 14195–14202.
93 X. Tian, H. Ma, Y. Gao and B. Xu, *J. Mater. Chem. A*, 2022, **10**, 14011–14019.
94 M. S. Javed, T. Najam, I. Hussain, M. Idrees, A. Ahmad, M. Imran, S. S. A. Shah, R. Luque and W. Han, *Adv. Energy Mater.*, 2022, **13**, 2202303.
95 L. Li, W. Liu, K. Jiang, D. Chen, F. Qu and G. Shen, *Nanomicro Lett.*, 2021, **13**, 100.
96 X. Chen, H. Zhang, Y. Gao, J. H. Liu, X. Cao, C. Zhan, S. Wang, J. Wang, S. X. Dou and D. Cao, *Carbon Neutral*, 2022, **1**, 159–188.
97 D. Sui, M. Wu, K. Shi, C. Li, J. Lang, Y. Yang, X. Zhang, X. Yan and Y. Chen, *Carbon*, 2021, **185**, 126–151.
98 Y. Wang and J. Niu, *Molecules*, 2023, **28**, 4470.
99 L. Lei, Z. Cao, J. Li, H. Hu and D. Ho, *ACS Appl. Energy Mater.*, 2022, **5**, 12790–12797.
100 M. Dong, Y. Mu, L. Zhou, Y. Zhao, X. Zhang, D. Tan, X. Pan and H. Wei, *J. Alloys Compd.*, 2023, 172846.
101 J. Zeng, L. Dong, L. Sun, W. Wang, Y. Zhou, L. Wei and X. Guo, *Nanomicro Lett.*, 2020, **13**, 19.
102 Y. Gu, T. Yu, P. Xue, Q. Zhang, S. Ma and X. Xu, *ChemElectroChem*, 2021, **8**, 4498–4508.
103 B. Anasori, M. R. Lukatskaya and Y. Gogotsi, *Nat. Rev. Mater.*, 2017, **2**, 16098.
104 C. Zhang, Y. Ma, X. Zhang, S. Abdolhosseinzadeh, H. Sheng, W. Lan, A. Pakdel, J. Heier and F. Nüesch, *Energy Environ. Mater.*, 2020, **3**, 29–55.
105 M. S. Javed, A. Mateen, S. Ali, X. Zhang, I. Hussain, M. Imran, S. S. A. Shah and W. Han, *Small*, 2022, **18**, 2201989.
106 H. Wang, Y. Xue, X. Song, S. Lei, H. Yu, C.-F. Du, Z. Ren, R. Guo and F. Zhou, *J. Mater. Chem. A*, 2022, **10**, 20953–20963.
107 W. Liu, L. Li, C. Hu, D. Chen and G. Shen, *Adv. Mater. Technol.*, 2022, **7**, 2200158.

108 H. Zhang, Z. Wei, J. Wu, F. Cheng, Y. Ma, W. Liu, Y. Cheng, Y. Lin, N. Liu, Y. Gao and Y. Yue, *Energy Storage Mater.*, 2022, **50**, 444–453.
109 Z. Cao, G. Hu, W. Feng, J. Ru and Y. Li, *Carbon Neutral*, 2023, **2**, 699–708.
110 B. Pal, S. Yang, S. Ramesh, V. Thangadurai and R. Jose, *Nanoscale Adv.*, 2019, **1**, 3807–3835.
111 C. Zhong, Y. Deng, W. Hu, J. Qiao, L. Zhang and J. Zhang, *Chem. Soc. Rev.*, 2015, **44**, 7484–7539.
112 T. Zhang, Y. Tang, S. Guo, X. Cao, A. Pan, G. Fang, J. Zhou and S. Liang, *Energy Environ. Sci.*, 2020, **13**, 4625–4665.
113 W. Liu, C. Hu, L. Li and G. Shen, *ACS Appl. Energy Mater.*, 2023, **6**, 7387–7394.
114 W. Zhang, F. Guo, H. Mi, Z. S. Wu, C. Ji, C. Yang and J. Qiu, *Adv. Energy Mater.*, 2022, **12**, 2202219.
115 S. Guo, L. Qin, T. Zhang, M. Zhou, J. Zhou, G. Fang and S. Liang, *Energy Storage Mater.*, 2021, **34**, 545–562.
116 D. Qi, Y. Liu, Z. Liu, L. Zhang and X. Chen, *Adv. Mater.*, 2017, **29**, 1602802.
117 Y. Cheng, Y. Xie, S. Yan, Z. Liu, Y. Ma, Y. Yue, J. Wang, Y. Gao and L. Li, *Sci. Bull.*, 2022, **67**, 2216–2224.



 